# Development of Pial Collaterals by Extension of Pre-existing Artery Tips

Suraj Kumar, Niloufer Shanavas, Swarnadip Ghosh, Vinayak Sivaramakrishnan, Manish Dwari, Soumyashree Das[#]

National Centre for Biological Sciences, Tata Institute of Fundamental Research, Bengaluru, KA 560065, India

[#] Corresponding author (soumyashree@ncbs.res.in)

**Key Words**

Pial Collateral Artery, Artery Endothelial Cell, Vascular Endothelial Growth Factor Receptor-2, Intra-vital Imaging, Genetic Lineage Tracing

## SUMMARY

Pial collaterals provide protection from ischemic damage and improve prognosis of stroke patients. The origin or precise sequence of events underlying pial collateral development is unclear and has prevented clinicians from adapting new vascularization and regeneration therapies. We use genetic lineage tracing and intra-vital imaging of mouse brains at cellular resolution to show that during embryogenesis, pial collateral arteries develop from extension and anastomoses of pre-existing artery tips, in a VegfR2 dependent manner. Our data demonstrate that an arterial receptor, Cxcr4, earlier shown to drive artery cell migration and coronary collateral development, is dispensable for formation and maintenance of pial collateral arteries. Our study reveals that collateral arteries of the brain are built by a unique mechanism, distinct from that of the heart.

## INTRODUCTION

Pial (leptomeningeal) collateral arteries are an extensive network of inter-artery anastomoses found in the pial layer of the brain. In humans, the extent of pial collateral circulation is a predictor of stroke outcome.[1,2] Stroke occurs when blood supply is obstructed to a part of the brain and is one of the leading causes of morbidity worldwide (World Health Organization).[3] Pial collaterals serve as an alternate route of blood flow and alleviate the symptoms of ischemic stroke by bypassing vascular occlusions. Thus, understanding mechanisms which drive the origin and remodelling of pial collateral arteries is of immense clinical relevance.

Results from preclinical studies indicate wide-spread variation in the pial collateral artery network among individuals and organs.[4] These variations are a result of differential expression and function of proteins associated with Vascular endothelial growth factor (Vegf) signalling axis.[5–7] Different mouse strains demonstrate differential Vegfa expression level which corelate with their pial collateral density.[8] Similarly, global overexpression of Vegf ligand increases number of native pial collaterals and improve collateral perfusion post-injury.[5,6] The receptor mediating the function of Vegf ligand during the formation of pial collaterals is Vegf receptor-2 (VegfR2).[6] A global knockdown of Vegf or VegfR2 during embryogenesis and in a time-frame when pial collaterals are expected to form, results in reduction in their number and diameter.[6] Thus, Vegf is a key driver of pial collateral formation and a critical factor which regulates variation in extent of pial vascular network in mice.

The vital role of Vegf in murine pial collateral development was discovered almost a decade ago.[5,6] However, it is still unclear how the various molecular players of Vegf pathway orchestrate the formation or remodelling of pial collateral network. In

mice, it is hypothesized that an *arteriole-specific sprouting angiogenesis like* process leads to the formation of the foremost pial collaterals.[6] However, molecular evidence supporting the identity of these sprouting cells (if arteries or capillaries) is missing. Additionally, the cellular origin or fate of these sprouts is unknown. Finally, the possibility of cooperation from other vascular processes, such as arterialization, arteriogenesis or artery-reassembly, in building pial collaterals, needs to be thoroughly investigated.

In this study, we use genetic lineage tracing in conjunction with live imaging of pial vasculature of transgenic mouse embryos and adults to understand mechanisms by which Vegf regulates pial collateral development and maintenance. Our data indicate that the cellular source of pial collateral arteries is primarily pre-existing artery endothelial cells (ECs) which build the first network of pial collaterals at embryonic day (e)15.5 via VegfR2-dependent artery tip extension. While arterial VegfR2 was essential for formation of pial collaterals *de novo*, it was dispensable for its maintenance through adulthood. Arterial Cxcr4 (C-X-C chemokine receptor type-4), which is critical for coronary artery formation in mice[9] was dispensable during pial collateral formation and its maintenance. Together, our data indicate that artery endothelial cells build collateral arteries by utilizing distinct vascular mechanisms in heart and brain.

## RESULTS

### Pial collateral arteries form during embryogenesis

We developed a whole brain imaging technique to reliably visualize all pial arteries (Figure **S1A**, **B**). Due to lack of unique markers, accurately identifying pial collateral arteries is exclusively dependent on their location. Pial collateral arteries

are artery segments which interconnect the ends of cerebral arteries and can be seen in the watershed region (Figure **S1B**). To acquire this spatial information, it was imperative to image the entire pial artery network. Our technique allowed us to precisely identify pial collateral arteries. We specifically focused on collateral arteries which connected and received blood flow from Anterior Cerebral Artery (ACA) and Middle Cerebral Artery (MCA), as the coverage of this arterial network is most extensive.

We first investigated the developmental stage when pial collaterals first appeared. Mouse brains were harvested at different developmental time points and whole brain immunostaining was performed for Connexin-40 (Cx40) protein, a known marker for mature artery endothelial cell. Analyses of pial arterial network in both hemispheres revealed the appearance of MCA at embryonic day e12.5 followed by ACA at e13.5 (Figure **S1C** and **S2A**, **B**). At e14.5, both cerebral arteries were present with no arterial connections between them (figure **S2C**). Subsequently, the first arterial anastomoses appeared at e15.5 (Figure **S2D**) which then remodelled to expand in number through birth/postnatal day (P)0 (Figure **S1C** and **S2D**-**F**). This method confirmed that both MCA and ACA are present at e14.5 (Figure **S2G**) and the foremost pial collaterals appear at e15.5 (Figure **S2H**).

To confirm the above results, we next used a knock-in mouse line (*Cx40*$^{eGFP/+}$) where eGFP expression was driven by *Cx40* promoter activity. Brains from different developmental stages confirmed our findings from Cx40 immunostaining. MCA appeared at e12.5, ACA appeared at e14.5 and collateral arteries between MCA and ACA appear at e15.5 (Figure **S3A**-**F** and **S1C**). eGFP$^{+}$ cerebral arteries (MCA and ACA) were formed by e14.5 (Figure **S3G**) and the first eGFP$^{+}$ collateral artery between MCA and ACA appeared at e15.5 (Figure **S3H**). Thus, using two

independent methods— Cx40 immunostaining and detecting its reporter activity, we demonstrate that mouse pial collateral arteries form during development, and appear precisely at e15.5 (Figure **S1C**).

**Intravital imaging reveals arterial origin of pial collaterals by artery tip extension**

Despite several hypotheses, there is lack of compelling data in support of vascular mechanisms which drive pial collateral development. Pial collaterals appear at late embryonic stages. At this developmental stage, rapid vascular changes make it difficult to distinguish collateral-specific events from overall vascular growth, thus making it challenging to draw information from fixed brain samples. Additionally, late embryonic stages cannot be cultured *ex vivo* due to extremely demanding metabolic and physiological needs. Thus, we custom-developed an imaging paradigm to perform intra-vital imaging of pial layer at late embryonic stages (e16-e17) (Figure **1A**), a developmental stage where the brain is actively building pial collaterals. Briefly, embryos of the desired developmental time points were dissected out (with their intact yolk sac) from the anesthetized pregnant dams while still connected to the mother via their umbilical cord. Embryos were maintained at 37˚C and immobilized at appropriate orientation to aid imaging. The embryos were subjected to stereoscopic or confocal imaging for several hours. This imaging set up allowed visualization of the entire hemisphere– MCA, ACA, and connected collateral arteries (Figure **1B**).

Pial collaterals appear only after the primary branches of MCA and ACA have developed (Figure **S1C**). We hypothesized that the branches of these cerebral arteries contribute towards formation of pial collaterals. To test this hypothesis,

121 *Cx40CreER; Rosa26$^{TdTomato}$*; *Tie2::eGFP::Claudin5* mice were used to label artery
122 ECs with TdTomato and all endothelial cells with eGFP. To activate TdTomato,
123 Tamoxifen was administered at e13.5, when both MCA and ACA are present and
124 would be labelled in 2 days, [9,10] by e15.5. Imaging of endothelial cells derived from
125 arteries was performed at e16-e17. This experimental strategy allowed visualization
126 of cellular dynamics specific to artery cells derived from pre-existing arteries (Figure
127 **1C**) and excluded the possibility of capturing other vascular processes.

128 We performed intra-vital time-lapse imaging of pial arteries and investigated if
129 pial collaterals originate from pre-existing artery endothelial cells. We focused on the
130 watershed region: an initial artery-free region which spans the distal ends of both
131 arterial trees (MCA and ACA) and is later occupied by pial collaterals (Figure **S1C**
132 and **1D**-**F**). Stereoscopic images of e16.5 brains revealed that branches from MCA
133 and ACA extend (arrowheads, Figure **1E**) and anastomose to build collaterals in the
134 pial watershed (brackets, Figure **1E**). Additionally, TdTomato expression in artery
135 tips (orange arrow, Figure **1E**) and collaterals (green arrow, Figure **1E**) increased
136 over time. These changes were executed within a short span of 80 minutes, and
137 could not have been captured in fixed brain samples.

138 We next investigated artery cell dynamics associated with the growth fronts of
139 the two cerebral arteries (Figure **1F**, **G**). At e16.5, the distal branches of the
140 developing MCA extended and anastomosed to build an artery network *de novo*
141 (arrowheads, Figure **1G**). This is the first evidence demonstrating that pre-existing
142 cerebral artery tips build pial collaterals. We then performed intra-vital time-lapse
143 confocal imaging of brains at e16, a stage prior to when we observed collateral
144 artery networks being built *de novo* (Figure **1E**, **G**). Confocal imaging at e16 provided
145 the necessary cellular resolution to quantitatively assess artery-tip extensions from

146 MCA and ACA branches (Figure **1H-J**). As expected, we clearly observed artery tip
147 extension of MCA branch (Figure **1H**, **I**) and the ACA branch (Figure **1H**, **J**) within an
148 hour. Additionally, we noted several artery-specific movements within the pial layer.
149 This included the appearance of single artery endothelial cells (arrows, Figure **S4A**,
150 **B**), movement of these single artery cells towards an artery (Figure **S4C**, **D**), and
151 emergence of arterial sprouts (arrowheads, Figure **S4A**, **B**). Most interestingly, all
152 artery cell movements were observed along microvascular tracks which appeared
153 structurally more organized/tubular than the surrounding capillaries (arrowheads,
154 Figure **1K** and Figure **S4A**, **E**). These "microvascular tracks" were distinct from the
155 surrounding capillary plexus in that they formed direct connections between two
156 arteries but were not entirely populated by TdTomato$^{+}$ artery derived endothelial
157 cells (Figure **1K** and Figure **S4A**, **E**). Together, for the first time, we provide direct
158 evidence for the vascular origin of pial collaterals— pre-existing MCA/ACA artery tips
159 grow on distinct microvascular paths and connect with each other to build pial
160 collaterals *de novo* (Figure **1L**).

161 **Artery ECs are the major cellular contributors of pial collaterals during**
162 **embryogenesis**

163 We next assessed the vascular-lineage composition of pial collaterals at a
164 later stage when the collateral artery network has fully formed. This would allow us
165 to: 1) determine if the artery cell contribution to nascent pial collaterals observed at
166 e16.5 (Figure **1E**) persisted in later stages and 2) check contribution from
167 microvascular lineage which is evident in newly formed collaterals in heart[9,11] and
168 skeletal muscle.[12] Genetic lineage tracing with *Cx40CreER; Rosa26$^{TdTomato}$* and
169 *ApjCreER; Rosa26$^{TdTomato}$* mice were performed where TdTomato expression could
170 be conditionally induced, with Tamoxifen, specifically in artery ECs or capillaries

171 respectively. Tamoxifen was administered to timed pregnant dams at e14.5 when
172 both MCA and ACA arteries are present (Figure **2A**, **S2G**, **S3G**). Embryos were
173 analysed at e18.5 or P0 when the pial collateral artery network has completely
174 formed (Figure **2A**, **S2H**, **S3H**). Whole embryonic brains were immunostained for
175 Cx40 and segments of collateral arteries between MCA and ACA were analysed for
176 lineage contribution (Figure **2B-J**).

177 We assessed the extent of lineage contribution from artery or capillary ECs
178 towards pial collaterals. As expected, all pre-existing artery ECs were labelled and
179 traced in *Cx40CreER; Rosa26*$^{TdTomato}$ embryos (Figure **2C**, **D**, **G**, **I**). Whole brain
180 imaging of the embryo (Figure **2C**) allowed identification of pial collateral arteries
181 present between MCA and ACA in the watershed (Figure **2D**). Individual collateral
182 segments as identified by Cx40 immunostaining were analysed for presence of
183 TdTomato$^{+}$ artery ECs (Figure **2D**, **G**, **I**). This analysis revealed that 77% of the
184 Cx40$^{+}$ collateral area to be TdTomato$^{+}$ (Figure **2B**). In contrast to this data, a similar
185 analysis in an independent experiment with *ApjCreER; Rosa26*$^{TdTomato}$ mice (Figure
186 **2E**, **F**, **H**, **J**) showed only 31.6% of the collateral area to be TdTomato$^{+}$, i.e. traced
187 from capillaries (Figure **2B**). Thus, artery ECs are the major contributors of pial
188 collateral arteries during development.

189

190 **Arterial VegfR2 mediates artery tip extension and is essential for pial collateral**
191 **artery development**

192 We analysed similarities, if any, in the molecular programs used by artery
193 endothelial cells during collateral development in the heart and brain. Post-injury,
194 neonatal coronary artery ECs undergo extensive migration and proliferation to build
195 new coronary collateral arteries in the watershed. The processes of artery cell

196 migration and proliferation are heavily dependent on Cxcr4[9] and VegfR2[13]
197 respectively. To assess the functions of Cxcr4 and VegfR2 in pial collateral
198 development, we deleted the respective genes at e14.5 and assessed the extent of
199 pial collateral network at e18.5/P0 by whole brain imaging (Figure **3A**). Surprisingly,
200 deletion of arterial *Cxcr4* did not affect the pial collateral network at e18.5 (Figure **3B**,
201 control=8, artery specific knockout for *Cxcr4*=13) or in adulthood (Figure **S5**, N=5 per
202 genotype). This data suggests that a Cxcr4-independent vascular mechanism
203 facilitates pial collateral development and its maintenance.

204 We next assessed if pial collateral artery development is dependent on
205 arterial VegfR2. Whole brain imaging of control and *VegfR2* artery specific knockout
206 embryos showed differences in collateral connectivity in the watershed, and required
207 systematic quantification (Figure **3C**-**F**). The extensive connectivity of pial arteries
208 across the hemisphere (including watershed) provide several possible collateral
209 paths for the blood to flow. These artery-artery connections are innumerable. We
210 developed a method that allowed us to compare the pial artery coverage between
211 the control and *VegfR2* artery EC specific knockout brains quantitatively (Figure **3C**).
212 Intensity line-profiles were generated across the width of the hemisphere (Figure **3C**
213 **i**, **ii**). The identified peaks per line-profile was plotted across the width of the
214 hemisphere (Figure **3C iii**). The data was fit to a gaussian function and the fitted
215 curves were used as representative of the arterial coverage per hemisphere in each
216 mouse (Figure **3C iv**). The average of the fitted curves represented one genotype
217 (grey curve, Figure **3C iv**). Quantification of pial artery coverage showed significantly
218 different distributions between control and *VegfR2* knockout brains (KS test, D
219 value=0.569, p value=2.2066 X $10^{-141}$) (Figure **3E**). Peak arterial coverage was
220 observed at the centre of the hemisphere and watershed was defined as a region ±

221 500μm from the centre (Figure **3E**). The loss of arterial coverage in the watershed
222 was evident in the knockout (Figure **3E**) and was quantified as area under the curve
223 (Figure **3E**, **F**). This area under the curve represented the extent of collateral artery
224 network in the watershed and was significantly lower in brains without arterial
225 *VegfR2* (Figure **3F**, unpaired t-test, p value= 0.0001). Thus, depletion of *VegfR2* from
226 arteries reduced the extent of pial collaterals formed during embryogenesis.

227 We next investigated the possible mechanisms by which arterial VegfR2
228 facilitated pial collateral formation. *VegfR2* was deleted from artery ECs at e14.5,
229 and analyses of pial collateral network was performed at e16.5 (Figure **3G**), a
230 timepoint when collaterals are beginning to form via artery tip extensions (Figure **1D-**
231 **G**)**.** Quantification showed fewer TdTomato$^{+}$ collateral arteries (i.e. TdTomato
232 contiguous or Td$^{con}$) without arterial *VegfR2* (Figure **3H**). This indicated that initiation
233 of collateral development at an earlier timepoint, e16.5, also depends on arterial
234 *VegfR2*. This VegfR2-dependent collateral phenotype (Figure **3H**) was independent
235 of artery cell proliferation which was minimal at this stage, for both control and
236 *VegfR2*-deleted brains (data not shown). Close analyses of collaterals in control
237 brains showed that TdTomato$^{+}$ artery cells occupied a major length of microvascular
238 tracks connecting branches of MCA and ACA (Figure **3I**). This observation was in
239 contrast to *VegfR2*-depleted brains where TdTomato$^{+}$ artery cells sparsely populated
240 the microvascular tracks (Figure **3J**). Thus, arterial VegfR2 regulates pial collateral
241 formation by promoting artery growth along microvascular tracks.

242 We investigated if endothelial cells of capillary lineage populate pial collaterals
243 via Dach1; a transcriptional factor that drives arterialization of capillaries into
244 coronary arteries during cardiac development in mice.[14] As observed in developing
245 mouse hearts,[14,15] expression of Dach1 was higher in capillaries as compared to

246 arteries (Figure **S6A**). *Dach1* was deleted from capillaries at e14.5 and the extent of
247 pial collateral network was assessed at e18.5 (Figure **S6B**). Interestingly, no
248 significant difference was observed in the number of Cx40$^{+}$ collaterals in the *Dach1*
249 capillary-EC specific knockout brains (Figure **S6C**). Thus, in contrast to heart, the
250 formation of pial collaterals during embryogenesis is independent of capillary Dach1
251 activity.

252 **Pial collaterals do not remodel in adulthood**

253 We next investigated the cellular dynamics associated with fully formed and
254 mature pial collateral arteries between MCA and ACA in adult mice. For this, we
255 utilized an extensive longitudinal in vivo imaging paradigm that allowed us to get
256 single cell resolution of vascular structures. 3-5 months old *Cx40CreER;*
257 *Rosa26$^{TdTomato}$*; *Tie2::eGFP::Claudin5* mice underwent craniotomy and an optical
258 window of 4mm was implanted on one of the hemispheres between the cranial
259 landmarks—bregma and lambda (Figure **4A**, **B**). In these transgenic mice, pre-
260 existing pial arteries were labelled with TdTomato upon Tamoxifen administration
261 (Figure **4C**), and constitutively expressing GFP marked all endothelial cells. 5
262 consecutive doses of Tamoxifen resulted in 95.4% and 86.8% recombination in
263 proximal and distal arteries respectively, but a lower 65.3% recombination in the pial
264 collateral regions (Figure **4D**). A lower recombination efficiency in the pial collateral
265 arteries resulted in a patchy reporter pattern comprising of a mixture of TdTomato$^{+}$
266 and TdTomato$^{-}$ cells (Figure **4D**). Like in developmental stages (Figure **2B**), artery
267 ECs populate adult pial collaterals to a greater extent as compared to other vascular
268 lineages. This ultimately allowed us to most accurately track the position of individual
269 cells within a given collateral artery.

270 An optical window allows longitudinal imaging. Imaging the collateral zone
271 (watershed between MCA and ACA) for a month (Figure **4E**), resulted in high quality
272 images with single cell resolution (Figure **4E**-**H**). Morphology of the pial vessels
273 alongside reporter activity in endothelial cells were instrumental in identifying pial
274 arteries, veins and capillaries (Figure **4E**, **I**). High resolution images of artery
275 endothelial cells (both TdTomato$^{+}$ GFP$^{+}$ and TdTomato$^{-}$ GFP$^{+}$) within a collateral
276 artery segment across many collaterals and optical windows were analysed (Figure
277 **4J**, **K**). Data showed that artery endothelial cells do not remodel or reposition
278 themselves within a given collateral artery segment (Figure **4J**-**M**). Cellular matrices
279 representative of the relative position of collateral artery cells suggested that under
280 physiological conditions, every artery cell within a mature/ adult pial collateral
281 maintains its contact with the same neighbouring cells (Figure **4L**, **M**). Thus,
282 surprisingly, the cellular organization within pial collaterals and the overall collateral
283 structure was extremely stable. For the first time our data, with cellular resolution,
284 demonstrates the static nature of artery endothelial cells during homeostasis.

285 **Arterial VegfR2 is dispensable for pial collateral maintenance**

286 We next asked if arterial VegfR2 is necessary for the maintenance of adult
287 pial collaterals using adult mice deficient in arterial *VegfR2*. Using the same in vivo
288 imaging paradigm mentioned above, pial collateral segments in artery endothelial
289 cell specific *VegfR2* knockout mice were imaged at cellular resolution and followed
290 for a month with imaging time-points separated by 2 weeks (Figure **5A**). Longitudinal
291 imaging through an optical window (Figure **5B**) yielded a map of vascular network
292 which could be followed for months (Figure **5C**, **D**). Of note, our qualitative
293 observation suggests that *VegfR2* depleted pial collaterals had smaller diameters.
294 High magnification images of watershed between MCA and ACA (Figure **5E**-**G**)

295 allowed us to analyse individual *VegfR2*$^{-/-}$ artery endothelial cells (TdTomato$^{+}$)
296 residing on adult collateral arteries (Figure **5H-J**). Long term imaging of the same
297 collateral regions across many collaterals and mice showed no significant changes in
298 cellular positions relative to their neighbouring cells (Figure **5K-M** and Figure **S7**).
299 Thus, arterial VegfR2 is dispensable for maintenance of mature pial collateral
300 arteries. Together, in this study, we highlight the essential role of arterial VegfR2 in
301 promoting artery-tip extension and pial collateral development during embryogenesis
302 (Figure **5N**); a function dispensable in adulthood.

303 **DISCUSSION**

304 In the present study, we investigate artery cell dynamics during collateral artery
305 formation and maintenance in mouse brain. Firstly, using an artery-specific
306 molecular marker, we dissect out where and when pial collaterals appear during
307 embryogenesis. Secondly, we develop a live imaging method in mouse embryos to
308 provide conclusive evidence that pre-existing arteries grow on pre-determined
309 microvascular tracks which then connect to build pial collaterals *de novo*. Thirdly, by
310 combining mouse genetics with whole brain confocal imaging at cellular resolution,
311 we show that an angiogenic vascular receptor VegfR2 facilitates artery-tip extension
312 on microvascular tracks and aids origin of pial collaterals. Finally, we show that
313 Cxcr4, a receptor essential for Artery Reassembly and formation of coronary
314 collateral arteries *de novo*, is dispensable for development of pial collaterals. Thus,
315 two fundamentally distinct mechanisms contribute to the origin of coronary and pial
316 collaterals.

317 **Organ-specific mechanisms build collaterals**

318 For the first time, we provide direct proof that a vascular mechanism driven
319 specifically by artery endothelial cells leads to the origin of pial collaterals. Like in the
320 heart, this artery specific process is regulated by arterial VegfR2, but is distinct from
321 Artery Reassembly where pre-existing artery cells dissociate from resident
322 coronaries, migrate, de-differentiate/proliferate and coalesce to build coronary
323 collaterals.[9,13] Instead, developing pial arteries extend along microvascular tracks
324 and connect with other artery tips to build new collateral artery paths. Furthermore, in
325 heart, coronary collateral formation is regulated by arterial Cxcr4 which drives artery
326 cell migration during Artery Reassembly. In contrast, arterial Cxcr4 had no impact on
327 pial collateral formation or its maintenance. Unlike heart, pial artery endothelial cells
328 contribute minimally via proliferation. Evidence for negligible artery cell proliferation
329 prompts us to hypothesize that artery endothelial cells at the distal ends experience
330 a forward push from the proximal parts of the artery. This forward pressure could be
331 generated due to incorporation of new cells or expansion of existing cells at the
332 proximal artery segments.

333 The need for functional collaterals is most during an ischemic condition such
334 as an artery occlusion, and can significantly impact tissue function. The differences
335 in factors which regulate origin of coronary and pial collaterals, are potentially driven
336 by the metabolic needs of these tissues. While cardiomyocytes can survive hypoxia
337 for few hours,[16] neurons are more susceptible to low levels of oxygen.[17] Higher
338 hypoxia sensitivity of brain tissue may lead to formation of pial collaterals during
339 embryogenesis as a protective measure, while coronary collaterals form only upon
340 induction of an arterial occlusion. Furthermore, collateral arteries in skeletal
341 muscle,[12,18] intestine,[19] and hind limb[20] can also undergo arteriogenesis.[21] Identifying

342 collateral-building vascular mechanisms across organs could reveal clinically
343 relevant information and open avenues for therapeutics.

344 **Arteries and capillaries collaborate to build collaterals**

345 We demonstrate the formation of collateral arteries, in real time, from pre-
346 existing arterial lineage as observed[9,10,13,22] or proposed[6] earlier. While this
347 manuscript was in progress, Perovic et al reported that two separate vascular
348 lineages populate pial collaterals.[10] We also observed that well-formed pial
349 collaterals are majorly populated by artery cells, and minimally by capillaries. Intra-
350 vital imaging of embryonic brains reveal that pre-existing artery cells extend along
351 defined microvascular paths to connect and build pial collaterals. These artery
352 specific events are executed within a short span, are difficult to capture using static
353 images and can be observed only by live imaging.

354 We cannot exclude the contribution of other artery-driven mechanisms. We
355 observed single artery cells migrating towards pre-existing arteries; coalescence of
356 these single cells with arteries could lead to arterial growth. Alternatively, the
357 migration and incorporation of single artery cells at the proximal ends of the artery
358 could indirectly contribute towards distal elongation of arteries. The dynamics of
359 single artery cell movements could also establish the branching pattern of the pial
360 artery network; the precise mechanisms for which are unknown.

361 We show that pre-existing artery tip extensions occur along a distinct
362 supporting structure. In the heart, single artery endothelial cells migrate by hitch-
363 hiking on to the capillary networks during the formation of new collaterals. On the
364 contrary, our study in the embryonic brains reveal the presence of a unique ($Tie2^{+}$)
365 vascular segment on which the arteries extend. These microvascular tracks are

366 distinct from the surrounding capillary mesh in that they anastomose ACA and MCA
367 arterial branches but do not show any artery specification. We speculate that the
368 microvascular tracks form during the specific time window (e16-e17) which coincides
369 with the period when majority of collaterals appear. Thus, these tracks may play a
370 crucial role in pial collateral formation. We hypothesize that the cellular origin of
371 these microvascular tracks is of capillary in nature. Elucidating the underlying
372 mechanism governing their formation and their molecular identity is an exciting
373 avenue for future investigation.

374 Our data about pre-defined microvascular tracks guiding the growth of pial
375 arteries suggest that the microvasculature could shape the artery network of the
376 brain. However, the microvascular contribution towards pial collaterals via
377 arterialization is less likely, as deletion of *Dach1*, a regulator of arterialization,[14,23]
378 had minimal effect on pial collateral network during embryogenesis. We propose that
379 as artery tips extend and get connected in the watershed, microvascular cells are
380 "trapped" within pial collaterals. This could generate a mixed lineage distribution[10]
381 within pial collaterals—both in embryos and adults. Together, multiple mechanisms
382 could be actively building pial vasculature during embryogenesis. That being said,
383 possible contribution from endothelial progenitor cells or peri-vascular cell types
384 (pericytes, smooth muscle cells) towards pial collateral formation cannot be entirely
385 excluded.

386 **Distinct mechanism for collateral maintenance**

387 Given that collateral arteries have a unique hemodynamic niche,[24] it would be
388 interesting to investigate which molecular programs maintain or remodel pial
389 collaterals in an adult brain. During embryogenesis, pial collaterals are built *de novo*,

390 in an artery-free zone and remodel as and when blood flows through them. In
391 contrast, mature collaterals remodel in response to differential blood flow patterns
392 and oxygen demands of their surrounding tissue. Postnatal remodelling of pial
393 collaterals is dependent on recruitment of smooth muscle cells and exhibits tortuous
394 morphology.[24] These fundamental differences could explain the requirement for
395 distinct molecular programs for building new collaterals and maintaining old ones.
396 This is evident in our study; VegfR2 controlled pial artery network during
397 embryogenesis but was dispensable in adulthood. That being said, arterial VegfR2
398 may regulate other aspects of vascular changes those require activation of
399 angiogenic pathways[25] such as remodelling induced by hypoxia, ischemia or aging.
400 We did not notice any remodelling events within adult pial collaterals, in presence or
401 absence of arterial Cxcr4. Together, adult pial collaterals are maintained via
402 mechanisms independent of two key angiogenic receptors in arteries—VegfR2 and
403 Cxcr4. It will be interesting to test if adult collateral maintenance is independent of
404 signals originating from an arterial niche. It is possible that surrounding
405 microvasculature plays a more prominent role in maintenance of pial arteries and
406 collaterals in adults. Investigating the molecular identity of the microvasculature
407 surrounding pial collaterals could reveal new vascular mechanisms key to collateral
408 maintenance.

409 **MATERIALS AND METHODS**

410 **Mouse lines**

| **Mouse lines** | **Source/ References** |
|---|---|
| *Rosa26$^{TdTomato}$* | The Jackson Laboratory, stock number 007909 |
| *Cx40CreER* | Miquerol et al. 2015[26] |

| | |
|---|---|
| *ApjCreER* | Chen et al. 2014[15] |
| *VegfR2 flox* | The Jackson Laboratory, stock number 018977 |
| *Cx40$^{eGFP/+}$* | Miquerol et al. 2004[27] |
| *Tie2::eGFP::Claudin5* | Knowland et al. 2014[28], Lutz et al. 2017[29] |
| *Cxcr4 flox* | The Jackson Laboratory, stock number 008767 |
| *Dach1 flox* | Chang et al. 2017[14] |

All experiments were performed on mice with mixed strain background. All mice were housed and bred at the National Centre for Biological Sciences animal facility in accordance with the Institutional Animal Ethics Committee (IAEC). All procedures were performed with approval from IAEC. Data shown in this study is compiled from age-matched males and females from several litters.

**Genotyping primer information**

| **Primer (F, forward; R, Reverse)** | **Sequence (5' → 3')** |
|---|---|
| Cre F | GCATTACCGGTCGATGCAACGAGTGATGAG |
| Cre R | GAGTGAACGAACCTGGAAATCAGTGCG |
| TdTomato mutant F | CTGTTCCTGTACGGCATGG |
| TdTomato mutant R | GGCATTAAAGCAGCGTATCC |
| TdTomato wild-type F | AAGGGAGCTGCAGTGGAGTA |
| TdTomato wild-type R | CCGAAAATCTGTGGGAAGTC |
| VegfR2 flox F | CCACAGAACAACTCAGGGCTA |
| VegfR2 flox R | GGGAGCAAAGTCTCTGGAAA |

| | |
|---|---|
| GFP F | GCACGACTTCTTCAAGTCCGCCATGCC |
| GFP R | GCGGATCTTGAAGTTCACCTTGATGCC |
| Cxcr4 flox F | CCACCCAGGACAGTGTGACTCTAA |
| Cxcr4 flox R | GATGGGATTTCTGTATGAGGATTAGC |
| Dach1 flox F | CTCCTGAAGATGAGGAGCTCACCCC |
| Dach1 flox R | AACAATTCTTGTCCTTCACGTGCCC |

418

419 **Visualization of pial arteries in fixed samples**

420 **Harvesting whole brains/heads from mouse embryos**

421

422 Depending on the developmental stages and size of the embryos, pial collateral
423 arteries were visualized either in whole brains (e18.5 or P0) or using whole heads
424 (e12.5- e16.5).

425

426 e12.5-e15.5: To perform the whole head explant at e12.5-e16.5 stages, the pregnant
427 females were euthanized through carbon dioxide overdose and a Y-shape incision
428 was made on the abdomen. Intact embryonic sacs were dissected out. Small
429 punctures were made on the embryo sac with the help of microforceps. The whole
430 embryo sac was fixed in 4% Paraformaldehyde (PFA) for 2 hours with gentle shaking
431 at 4°C. Following fixation, the embryo sac was washed at 4°C with gentle shaking.
432 This washing step was performed with 1X PBS and repeated 4 times every 15-20
433 mins. The embryos were then extracted from the embryo sacs and the heads were
434 removed with the help of microforceps.

435 e16.5: The embryonic explant at e16.5 is performed similarly. However, for
436 *Tie2::eGFP::Claudin5* genotype, the loose skin on top of the brain was removed to
437 aid immunostaining. Whole heads were imaged within 4 hrs, prior to PFA fixation to
438 avoid loss of GFP fluorescence signal.
439
440 e18.5: To perform the whole brain explant at e18.5 stage, the timed pregnant
441 females were euthanized as above. The skull of each embryo was gently removed
442 using the microforceps. The embryonic brains were scooped out with the help of a
443 microspatula and fixed in 4% PFA at 4°C for 2.5 hours. Agitation was avoided at this
444 stage to preserve tissue integrity of embryonic brains. The fixed embryonic brains
445 were then washed with 1X PBS three times at 15 minutes intervals with gentle
446 shaking at 4°C.
447
448 P0: Neonatal explants at P0 were performed by euthanizing the pups through carbon
449 dioxide overdose followed by decapitation. The skull was removed using scissors
450 and microforceps. The brains were scooped out using the microspatula. The brains
451 were then fixed with 4% PFA at 4°C for 2 hrs followed by three washes with 1X PBS
452 at an interval of 15 mins.
453
454 **Whole brain/head immunostaining of mouse embryos**
455
456 e12.5-e15.5: The embryonic heads (e12.5 - e15.5) were incubated in 0.1% PBST
457 (0.1% TritonX-100 in 1X PBS) for 2.5 hours to permeabilize the tissue, followed by
458 incubation with primary antibodies overnight at 4°C with gentle shaking. Heads were
459 then washed with 1X PBS, changing the buffer every 1-2 hours for 1 day. This step

460 was followed by incubation with secondary antibodies made in 0.1% PBST. Samples
461 were then washed every 1-2 hours for 1 day with 1X PBS. Following immunostaining
462 the brains are immersed in an anti-fade mounting media (from Jackson
463 ImmunoResearch Laboratories Inc.) and imaged immediately.
464
465 The embryonic and neonatal brains were incubated with primary antibody (made in
466 1X PBS) overnight, at 4°C with gentle shaking. Samples were then washed with 1X
467 PBS, changing the buffer every 1-2 hours for 1 day and incubated with Alexa Fluor
468 conjugated secondary antibodies (made in 1X PBS). Finally, samples were washed
469 every 1-2 hours for 1 day with 1X PBS and stored in mounting media or imaged
470 immediately.
471
472 Antibodies used are: Cx40 (Catalog number: Cx40-A, Alpha Diagnostics, 1:500
473 dilution), Dach1 (Catalog number: 10194-1-AP, Proteintech, 1:500 dilution), VegfR2
474 (Catalog number: AF644, R&D Systems, 1:250). All secondary antibodies were
475 procured from Invitrogen and used at a dilution of 1:500.
476
477 **Imaging whole brains/heads of mouse embryos**
478
479 The mice heads and brains from different developmental time-points were imaged
480 using Olympus FV-3000 upright or inverted confocal microscope by placing the
481 sample in a 2-well chamber Catalog number: 154461; Nunc™ Lab-Tek™ II Chamber
482 Slide™ System; Thermofisher Scientific. Whole brains and heads were scanned
483 using 4X and 10X air objectives, and multiple stacks were captured. The captured

484 image stacks were processed in ImageJ and stitched together using Adobe
485 Photoshop software.
486
487 The embryonic heads at e16.5 was imaged using Olympus FV-3000 5L Upright
488 microscope. The pre-fixed embryonic heads were attached to a 35mm plastic petri
489 dish using agarose gel prior to imaging. The whole head imaging was performed
490 using 4X air objective and watershed images were captured with 20X water
491 dipping/immersion objective and 1.5X optical zoom with brains immersed in 1X PBS.
492

493 **Visualization of pial arteries in live mice**

494 **In vivo imaging of embryonic pial arteries**

495 Immobilization of live embryo: *Cx40CreER; Rosa26$^{TdTomato}$*; *Tie2::eGFP::Claudin5*
496 pregnant dams with embryos at developmental stages between embryonic day
497 (e)16-e17 were anesthetized with a subcutaneous injection of Ketamine-Xylazine
498 (Ketamine (80 mg/kg); Xylazine (5 mg/kg)) cocktail. The dams were then placed in a
499 supine position on a regulated heating pad (TC1000, CWE) that was positioned on
500 top of a 3D-printed baseplate (as shown in Figure **1A**). A small incision was placed
501 along the midline of the abdomen. With a gentle retraction of the abdominal skin and
502 wall, a single uterine horn within the abdominal cavity was isolated. The uterus was
503 surgically opened and a single embryo along with the yolk sac was isolated and
504 placed into a 35mm petri dish. The embryo still connected to the dam was
505 immobilized by submerging the bottom part with 1% agarose, as shown in Figure **1A**.
506 The immobilized embryo is then submerged in dissection media (DMEM/F12 + 10%
507 FBS, Catalog number: 21041025, Thermo Fisher Scientific), and the media is

508 maintained at 37°C using a custom-made Arduino controlled media heating and
509 circulating device.
510
511 Live embryonic imaging: The setup along with anesthetized dam was placed under
512 Macro Zoom microscope MVX10-Olympus for large scale imaging and under
513 FV3000 upright confocal Microscope-Olympus for high resolution imaging using 20X
514 water dipping objective. In Macro Zoom Microscopy, the entire observable depth was
515 scanned whilst obtaining videos of 1 minute spanning a duration >2 hours in a time-
516 lapse manner. In confocal microscopy, the entire observable depth was scanned
517 with a step size of 1 micron. A total of 4 embryos were imaged under the Macro
518 zoom microscope and 5 embryos were imaged using confocal microscope. Out of
519 these embryos, the artery cell dynamics was captured in 2 brains from each
520 category.
521
522 Image processing: Image stacks obtained from Macro zoom microscopy was
523 registered using ImageJ plugin (*StackReg*) and the registered stack was de-
524 convolved using ImageJ plugin (*DeconvolutionLab2*) and finally maximum intensity
525 projection was obtained as shown in Figure **1D**. The image stacks obtained from the
526 confocal microscopy were processed similarly except the deconvolution step.
527
528 The MCA and ACA growth fronts were automatically traced and the length of the
529 traced path was measured using Simple Neurite Tracer (SNT). The distance of
530 single cells from an artery was measured manually using ImageJ.
531
532 **In vivo imaging adult pial arteries**

533 Craniotomy: *Cx40CreER; Rosa26$^{TdTomato}$; Tie2::eGFP::Claudin5 and*
534 *VegfR2$^{flox/flox}$;Cx40CreER; Rosa26$^{TdTomato}$;Tie2::eGFP::Claudin5* adult mice (3-5
535 months) underwent craniotomy to obtain optical access to the pial layer of the brain.
536 Mice were anesthetized under 2% Isoflurane (Abbott, North Chicago, IL, USA) and
537 were placed on a stereotaxic mount (Item number 51547; Stoelting, Wood Dale, IL,
538 USA) with the skull held tightly using ear bars. The mice were kept anesthetized with
539 2% Isoflurane using a nose-cone. 5mg/kg Dexamethasone in 1X PBS was
540 administered subcutaneously and the mice kept warm using a heating pad (TC1000,
541 CWE). The eyes were covered with an eye ointment and the hair above the skull
542 removed using a hair trimmer. The surgical area was thoroughly wiped clean with
543 70% ethanol. Sterile surgical tools were used for the surgery. A small incision was
544 made using a scalpel blade and the exposed skin was removed. The connective
545 tissue covering the skull in the exposed area was scraped off using scalpel blade
546 and Q-tips. Using a high-speed electrical drill (burr of diameter ~0.25mm), a window
547 of ~4mm diameter was carefully etched on the skull. The skull within the window was
548 eventually detached from the rest of the skull after repeated drilling and was carefully
549 lifted using a pair of fine forceps (Catalog number: 11255-20, Dumont #55) without
550 damaging the dura. During the process of drilling, the skull was constantly irrigated
551 with cortex buffer (Concentration; in mM: NaCl–125, KCl–5, glucose–10, HEPES–10,
552 $CaCl_2$–2 and $MgCl_2$–2. pH set to 7.35).[30] The exposed dura was aspirated with
553 cortex buffer until there is no bleeding and the window looked clear. An optical plug
554 made up of two 4 mm coverslip and one 5 mm coverslip (CS-5R & CS-4R; Warner
555 Instruments, Hamden, CT, USA) glued together (with NOA 68, Norland Optical
556 Adhesive) was placed on the exposed dura. The optical plug was gently pressed
557 using a toothpick such that the 5mm cover slip was touching the skull bone and then

558 cyano-acrylic glue was applied across the perimeter of the 5mm coverslip attaching it
559 to the skull. At this stage we had an optical window of 4mm. An aluminium head bar
560 with circular hole of 8mm was placed onto the skull aligned to the previously made
561 optical window. Next, dental cement (Catalog number 56877, 3M Relyx U200) was
562 applied over the exposed skull using a sterile toothpick while being careful to not get
563 it on the optical window. Once the dental cement was completely dry, the animal was
564 placed on a warm pad in a clean recovery cage. Animals undergoing craniotomy
565 were maintained on meloxicam (2 mg/kg) and enrofloxacin (5 mg/Kg body weight)
566 for 3-4 days until full recovery. Mice were further allowed to recover for at least 2
567 weeks post-surgery before the start of any experiment. Mice with an optical window
568 can be imaged longitudinally for 2-3 months until the optical window starts to lose its
569 clarity.
570
571 Live Adult Imaging: To perform in vivo imaging, mice were anesthetized through
572 intraperitoneal injection of Ketamine (80mg/Kg body weight) – Xylazine (5mg/Kg
573 body weight) cocktail. The eyes were covered with an eye ointment and the mice
574 were placed onto a custom-made baseplate and immobilized using the implanted
575 metal head plate to this baseplate. A heating pad (37°C) was placed under the
576 mouse to maintain the body temperature. Subsequently, the baseplate was placed
577 on a motorized XY-table of an upright confocal microscope (FV3000 upright confocal
578 Microscope-Olympus). The entire optical window was imaged using 10X air objective
579 (0.4 NA) and selected pial regions with collateral arteries were imaged with 20X
580 water dipping objective (0.5 NA). A total of N=3 adult mice per group (control and
581 *VegfR2* artery endothelial specific knockout) were imaged longitudinally for a period
582 of 1 month.

583

584 Image processing: The 10X image stacks obtained from the confocal microscopy of
585 the cranial window were registered using ImageJ plugin (*StackReg*) and maximum
586 intensity projection was obtained. The region of interest from the 20X image stacks
587 were cropped out slice by slice and stitched in Adobe Photoshop to avoid the
588 overlaying microvascular network in order to focus on the pial collaterals.

589 **Quantifications**

590 **Lineage contribution towards pial collaterals during embryogenesis**

591 Cx40 immunostained pial collateral segments from either *Cx40CreER;*
592 *Rosa26*$^{Tdtomato}$ or *ApjCreER; Rosa26*$^{TdTomato}$ brains were imaged at 10X with 2.12
593 optic zoom. Regions of interest were manually drawn to mark the collateral artery
594 segments. Lineage contribution was determined by quantifying TdTomato$^{+}$ coverage
595 on the collateral segment. This was performed by thresholding the images with Otsu
596 algorithm in ImageJ. The area fraction of the TdTomato$^{+}$ area per collateral segment
597 was calculated using the Measure tool in ImageJ. Contribution of the artery and
598 capillary derived ECs in collaterals was quantified by calculating the percentage of
599 collateral area covered by TdTomato$^{+}$ signal. 45 collateral segments (of an
600 approximate length of 600-800μm) from 7 *Cx40CreER*-lineage traced brains and 57
601 collateral segments from 8 *ApjCreER*-lineage traced brains were analysed.

602 **Number of collateral arteries per hemisphere**

603 In *Cx40CreER* TdTomato labelled brains, the collateral number was quantified based
604 on the number of contiguous TdTomato$^{+}$ vessels (Td-contiguous) connecting MCA
605 and ACA. Data shown in Figure **3H** was summarized from 2 control and 3 artery-

606 specific *VegfR2* knockout. Data shown in Figure **S2H** was summarized from e13.5
607 (N=5), e14.5 (N=5), e15.5 (N=5), e18.5 (N=5) and P0 (N=5) embryos and neonates.
608 Data shown in Figure **S3H** was summarized from e13.5 (N=3), e14.5 (N=3), e15.5
609 (N=2), e18.5 (N=2) and P0 (N=5) embryos and neonates. Data shown in Figure **S6C**
610 is quantified by counting number of Cx40 immunostained collateral arteries between
611 MCA and ACA, and is summarized from 4 control and 7 *Dach1* capillary specific
612 knockouts. An unpaired t-test was done to test significance statistically.

613 **Efficiency of TdTomato recombination**

614 Segments of collateral arteries, proximal arteries (PA) and distal arteries (DA) from
615 the image stacks taken with 20X objective were obtained from live adult imaging of
616 *Cx40CreER*; *Rosa26*$^{TdTomato}$; *Tie2::eGFP::Claudin5* mice. TdTomato$^{+}$ and TdTomato$^{-}$
617 cells were counted in each artery segment. Each segment was of an approximate
618 length of 600-800μm.The recombination efficiency was measured as ratio of
619 TdTomato$^{+}$ cells and total number of cells in the segment. A total of 10 collateral
620 segments, 10 PA segments and 10 DA segments from 4 mice were analysed to
621 obtain the recombination efficiency of TdTomato. One-way ANOVA was done to test
622 significance statistically (mean comparison Tukey test, PA vs. collateral, $p<0.0001$;
623 DA vs. collateral, $p<0.0001$; PA vs. DA, $p=0.08$).

624 **Pial artery coverage in whole brains and in the collateral zone**

625 The image stacks were obtained using confocal imaging of whole embryonic brains
626 with 10X objective, stitched using ImageJ plugin (*Stitching*) and max intensity
627 projection (MIP) was obtained. The MIPs were used for further analysis wherein one
628 complete hemisphere was cropped out and aligned vertically to the major axis of its

own elliptical boundary. Using a custom ImageJ macro, a line of the length of the major axis was scanned across the width of the image and intensity profile for every pixel along the horizontal axis was generated. Total number of local maxima (peaks) for each intensity profile was obtained using the built-in ImageJ macro function *Array.findMaxima (array, tolerance). The* tolerance used was 2 times the average background intensity. The number of peaks thus obtained was plotted across the width and the plot was fitted to a Gaussian function using OriginPro 2023b. The fitted curve was used as a representative of the arterial coverage per hemisphere. The fit curves obtained from various mice were aligned based on the Gaussian peaks and averaged to get the representative curves for various experimental groups. We considered a region of 1mm (-0.5mm to +0.5 mm) across the Gaussian peak as the collateral zone (watershed). The area under the curve within this region was used as a measure for the extent of the collateral network. 9 hemispheres from 9 embryos (e18.5) were analysed per group (control and artery-specific knockout for *VegfR2*). To test the statistical significance of the differences observed in pial artery coverage (Figure **3E**), a Kolmogorov-Smirnov (KS) test was done. D value= 0.569, p value= $2.2066 \times 10^{-141}$. To test the statistical significance of the area under the curve (pial collateral artery network shown in Figure **3F**), an unpaired t-test was done (p=0.0001).

## AUTHORS CONTRIBUTION

SD conceived the idea and designed the experiments. SK performed intravital imaging of embryos and adults. NS, SG, VS, MD performed other embryonic experiments. SD, SK, NS, SG wrote the manuscript. All authors contributed to editing the manuscript.

653 **ACKNOWLEDGEMENTS**

654 We thank the following facilities for their technical support: Animal Care and
655 Resource Center at NCBS, Mouse Genome Engineering Facility at NCBS, Central
656 Imaging and Flow Cytometry Facility at NCBS. We sincerely thank Dr. Dritan Agalliu
657 (Columbia University) and Dr. Kristy Red-Horse (Stanford University) for generously
658 sharing *Tie2::eGFP::Claudin5* and *Dach1*$^{fl/fl}$ mice respectively. We thank our funding
659 sources. This work is supported by NCBS/TIFR core funding and DBT/Wellcome
660 Trust India Alliance Intermediate Fellowship to SD (IA/I/20/2/505205). SK is
661 supported by DBT/Wellcome Trust India Alliance Intermediate Fellowship to SD. NS
662 and VS were supported by DBT INSPIRE Scholarship for Higher Education (SHE).

663 **DECLARATION OF INTERESTS**

664 None

665 **REFERENCES**

666 1. Lima, F.O., Furie, K.L., Silva, G.S., Lev, M.H., Camargo, E.C.S., Singhal, A.B.,
667 Harris, G.J., Halpern, E.F., Koroshetz, W.J., Smith, W.S., et al. (2010). The
668 pattern of leptomeningeal collaterals on CT angiography is a strong predictor
669 of long-term functional outcome in stroke patients with large vessel intracranial
670 occlusion. Stroke *41*, 2316–2322. 10.1161/STROKEAHA.110.592303.

671 2. Maas, M.B., Lev, M.H., Ay, H., Singhal, A.B., Greer, D.M., Smith, W.S., Harris,
672 G.J., Halpern, E., Kemmling, A., Koroshetz, W.J., et al. (2009). Collateral
673 vessels on CT angiography predict outcome in acute ischemic stroke. Stroke
674 *40*, 3001–3005. 10.1161/STROKEAHA.109.552513.

675 3. World Health Organisation. The top 10 causes of death
676 https://www.who.int/news-room/fact-sheets/detail/the-top-10-causes-of-death.

677 4. Zhang, H., Prabhakar, P., Sealock, R., and Faber, J.E. (2010). Wide genetic
678 variation in the native pial collateral circulation is a major determinant of
679 variation in severity of stroke. J. Cereb. Blood Flow Metab. *30*, 923–934.
680 10.1038/jcbfm.2010.10.

681 5. Clayton, J.A., Chalothorn, D., and Faber, J.E. (2008). Vascular endothelial
682 growth factor-a specifies formation of native collaterals and regulates collateral
683 growth in ischemia. Circ. Res. *103*, 1027–1036.
684 10.1161/CIRCRESAHA.108.181115.

685 6. Lucitti, J.L., MacKey, J.K., Morrison, J.C., Haigh, J.J., Adams, R.H., and Faber,
686 J.E. (2012). Formation of the collateral circulation is regulated by vascular
687 endothelial growth factor-a and a disintegrin and metalloprotease family
688 members 10 and 17. Circ. Res. *111*, 1539–1550.
689 10.1161/CIRCRESAHA.112.279109.

690 7. Lucitti, J.L., Sealock, R., Buckley, B.K., Zhang, H., Xiao, L., Dudley, A.C., and
691 Faber, J.E. (2016). Variants of Rab GTPase-Effector Binding Protein-2 Cause
692 Variation in the Collateral Circulation and Severity of Stroke. Stroke *47*, 3022–
693 3031. 10.1161/STROKEAHA.116.014160.

694 8. Chalothorn, D., Clayton, J.A., Zhang, H., Pomp, D., and Faber, J.E. (2007).
695 Collateral density, remodeling, and VEGF-A expression differ widely between
696 mouse strains. Physiol. Genomics. *30*, 179–191.
697 10.1152/PHYSIOLGENOMICS.00047.2007.

698 9. Das, S., Goldstone, A.B., Wang, H., Farry, J., D'Amato, G., Paulsen, M.J.,
699 Eskandari, A., Hironaka, C.E., Phansalkar, R., Sharma, B., et al. (2019). A
700 Unique Collateral Artery Development Program Promotes Neonatal Heart
701 Regeneration. Cell *176*, 1128-1142.e18. 10.1016/J.CELL.2018.12.023.

702 10. Perovic, T., Hollfinger, I., Mayer, S., Lips, J., Dopatka, M., Harms, C., and
703 Gerhardt, H. (2023). Pial collaterals develop through mosaic colonization of
704 capillaries by arterial and microvascular endothelial cells. bioRxiv,
705 2023.10.09.561542. 10.1101/2023.10.09.561542.

706 11. Jamaiyar, A., Juguilon, C., Wan, W., Richardson, D., Chinchilla, S., Gadd, J.,
707 Enrick, M., Wang, T., McCabe, C., Wang, Y., et al. (2022). The essential role
708 for endothelial cell sprouting in coronary collateral growth. J. Mol. Cell. Cardiol.
709 *165*, 158–171. 10.1016/j.yjmcc.2022.01.005.

710 12. Gabhann, F. Mac, and Peirce, S.M. (2010). Collateral Capillary Arterialization
711 following Arteriolar Ligation in Murine Skeletal Muscle. Microcirculation *17*,
712 333–347. 10.1111/J.1549-8719.2010.00034.X.

713 13. Arolkar, G., Kumar, S.K., Wang, H., Gonzalez, K.M., Kumar, S., Bishnoi, B.,
714 Rios Coronado, P.E., Woo, Y.J., Red-Horse, K., and Das, S. (2023).
715 Dedifferentiation and Proliferation of Artery Endothelial Cells Drive Coronary
716 Collateral Development in Mice. Arterioscler. Thromb. Vasc. Biol. *43*, 1455–
717 1477. 10.1161/ATVBAHA.123.319319.

718 14. Chang, A.H., Raftrey, B.C., D'Amato, G., Surya, V.N., Poduri, A., Chen, H.I.,
719 Goldstone, A.B., Woo, J., Fuller, G.G., Dunn, A.R., et al. (2017). DACH1
720 stimulates shear stress-guided endothelial cell migration and coronary artery

721 growth through the CXCL12-CXCR4 signaling axis. Genes. Dev. *31*, 1308–
722 1324. 10.1101/GAD.301549.117/-/DC1.

723 15. Chen, H.I., Sharma, B., Akerberg, B.N., Numi, H.J., Kivelä, R., Saharinen, P.,
724 Aghajanian, H., McKay, A.S., Bogard, P.E., Chang, A.H., et al. (2014). The
725 sinus venosus contributes to coronary vasculature through VEGFC-stimulated
726 angiogenesis. Development *141*, 4500–4512. 10.1242/dev.113639.

727 16. Scott Budinger, G.R., Duranteau, J., Chandel, N.S., and Schumacker, P.T.
728 (1998). Hibernation during Hypoxia in Cardiomyocytes ROLE OF
729 MITOCHONDRIA AS THE $O_2$ SENSOR. J. Biol. Chem. *273*, 3320–3326.
730 10.1074/jbc.273.6.3320.

731 17. Rink, C., and Khanna, S. (2011). Significance of Brain Tissue Oxygenation and
732 the Arachidonic Acid Cascade in Stroke. https://home.liebertpub.com/ars *14*,
733 1889–1903. 10.1089/ARS.2010.3474.

734 18. Mannion, J.D., Buckman, P.D., Magno, M.G., and Dimeo, F. (1992). Collateral
735 blood flow from skeletal muscle to normal myocardium. J. Surg. Res. *53*, 578–
736 587. 10.1016/0022-4804(92)90258-2.

737 19. Crissinger, K.D., and Neil Granger, D. (1988). Characterization of Intestinal
738 Collateral Blood Flow in the Developing Piglet. Pediatr. Res. *24*, 473–476.
739 10.1203/00006450-198810000-00011.

740 20. Kochi, T., Imai, Y., Takeda, A., Watanabe, Y., Mori, S., Tachi, M., and
741 Kodama, T. (2013). Characterization of the Arterial Anatomy of the Murine
742 Hindlimb: Functional Role in the Design and Understanding of Ischemia
743 Models. PLoS One *8*, e84047. 10.1371/JOURNAL.PONE.0084047.

744 21. Gao, Y., Aravind, S., Patel, N.S., Fuglestad, M.A., Ungar, J.S., Mietus, C.J., Li,
745 S., Casale, G.P., Pipinos, I.I., and Carlson, M.A. (2020). Collateral
746 Development and Arteriogenesis in Hindlimbs of Swine After Ligation of
747 Arterial Inflow. J. Surg. Res. *249*, 168–179. 10.1016/J.JSS.2019.12.005.

748 22. He, L., Liu, Q., Hu, T., Huang, X., Zhang, H., Tian, X., Yan, Y., Wang, L.,
749 Huang, Y., Miquerol, L., et al. (2016). Genetic lineage tracing discloses
750 arteriogenesis as the main mechanism for collateral growth in the mouse
751 heart. Cardiovasc. Res. *109*, 419–430. 10.1093/CVR/CVW005.

752 23. Raftrey, B., Williams, I.M., Rios Coronado, P.E., Fan, X., Chang, A.H., Zhao,
753 M., Roth, R., Trimm, E., Racelis, R., D'amato, G., et al. (2021). Dach1 Extends
754 Artery Networks and Protects Against Cardiac Injury. Circ. Res. *129*, 702–716.
755 10.1161/CIRCRESAHA.120.318271.

756 24. Zhang, H., Chalothorn, D., and Faber, J.E. (2019). Collateral Vessels Have
757 Unique Endothelial and Smooth Muscle Cell Phenotypes. Int. J. Mol. Sci. *20*,
758 3608. 10.3390/IJMS20153608.

759 25. Stanca Melincovici, C., Boşca, A.B., Şuşman, S., Mărginean, M., Mihu, C.,
760 Istrate, M., Moldovan, I.-M., Roman, A.L., and Mihu, C.M. (2018). Vascular
761 endothelial growth factor (VEGF)-key factor in normal and pathological
762 angiogenesis. Rom. J. Morphol. Embryol. *59*, 455-467.

763 26. Miquerol, L., Thireau, J., Bideaux, P., Sturny, R., Richard, S., and Kelly, R.G.
764 (2015). Endothelial plasticity drives arterial remodeling within The endocardium
765 after myocardial infarction. Circ. Res. *116*, 1765–1771.
766 10.1161/CIRCRESAHA.116.306476.

767 27. Miquerol, L., Meysen, S., Mangoni, M., Bois, P., van Rijen, H.V.M., Abran, P.,
768 Jongsma, H., Nargeot, J., and Gros, D. (2004). Architectural and functional
769 asymmetry of the His–Purkinje system of the murine heart. Cardiovasc. Res.
770 *63*, 77–86. 10.1016/j.cardiores.2004.03.007.

771 28. Knowland, D., Arac, A., Sekiguchi, K.J., Hsu, M., Lutz, S.E., Perrino, J.,
772 Steinberg, G.K., Barres, B.A., Nimmerjahn, A., and Agalliu, D. (2014).
773 Stepwise Recruitment of Transcellular and Paracellular Pathways Underlies
774 Blood-Brain Barrier Breakdown in Stroke. Neuron *82*, 603–617.
775 10.1016/j.neuron.2014.03.003.

776 29. Lutz, S.E., Smith, J.R., Kim, H., Bates, J.M., Gandhi, S.P., and Agalliu, D.
777 (2017). Caveolin1 Is Required for Th1 Cell Infiltration, but Not Tight Junction
778 Remodeling, at the Blood-Brain Barrier in Autoimmune Neuroinflammation.
779 CellReports *21*, 2104–2117. 10.1016/j.celrep.2017.10.094.

780 30. Holtmaat, A.J.G.D., Trachtenberg, J.T., Wilbrecht, L., Shepherd, G.M., Zhang,
781 X., Knott, G.W., and Svoboda, K. (2005). Transient and Persistent Dendritic
782 Spines in the Neocortex In Vivo. Neuron *45*, 279–291.
783 10.1016/j.neuron.2005.01.003.

784

785

786

787

## Main figures and figure legends

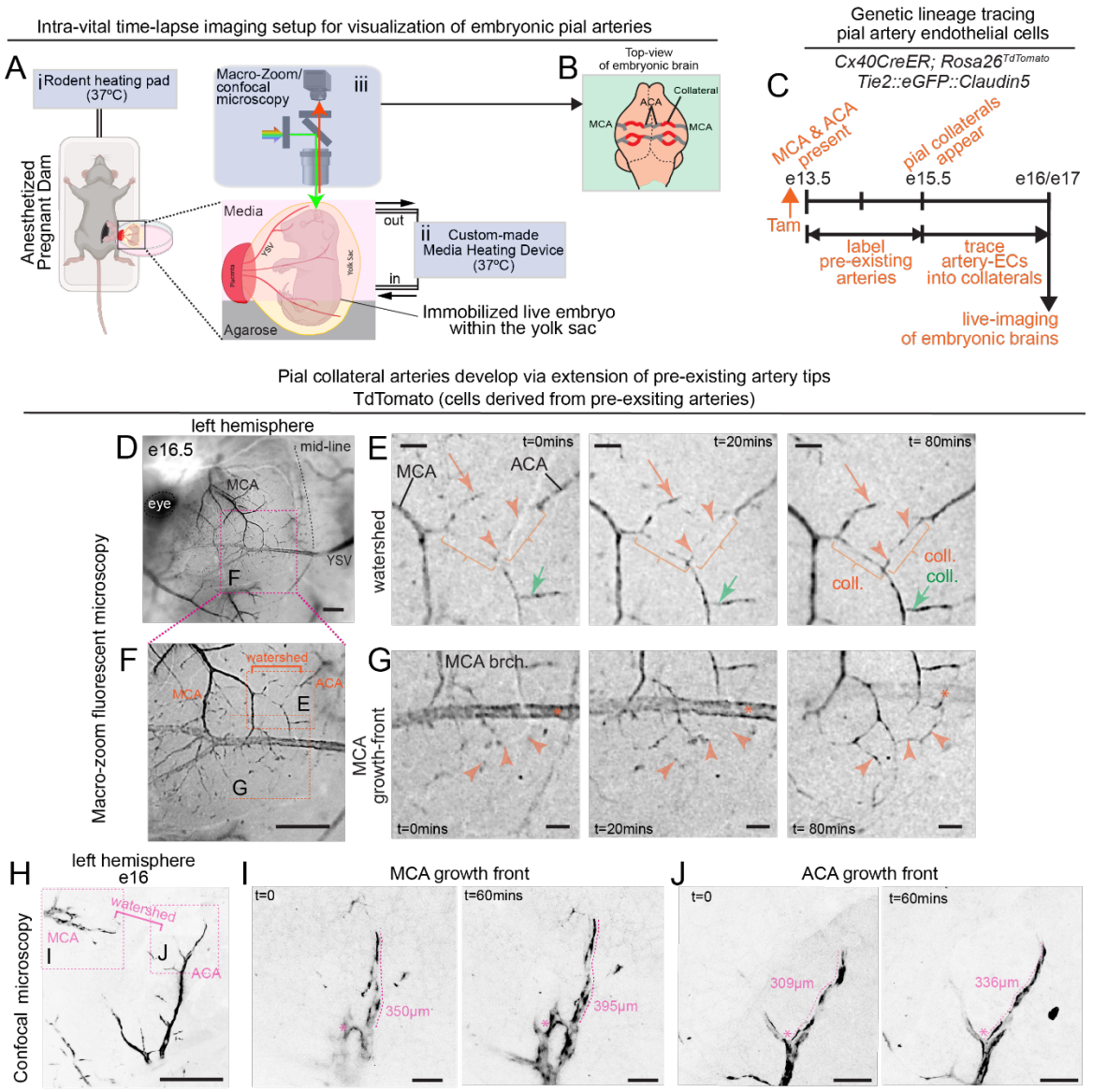


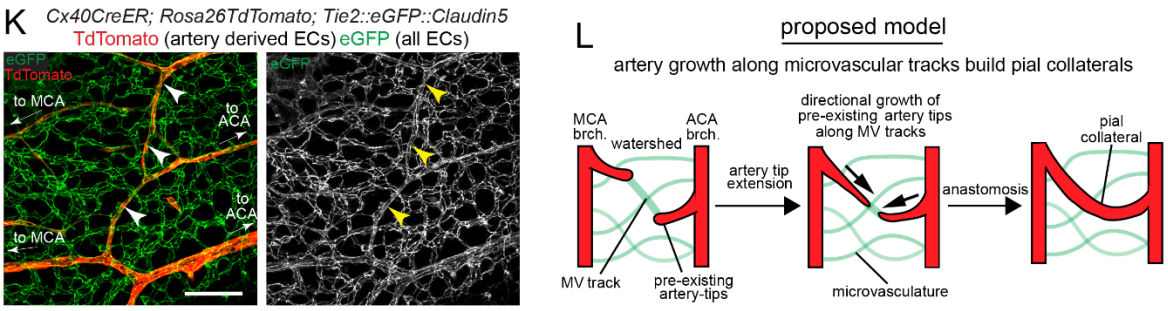

792 **Figure 1: Live imaging of embryonic pial vasculature**

793 (**A**) Intra-vital imaging set up to visualize the developing pial vasculature in mouse
794 embryos. **i** heating pad to maintain body temperature of anaesthetized pregnant dam
795 at 37°C. **ii** custom-built media heating device which also circulates dissection media
796 at 37°C **iii** shows macro-zoom or confocal microscopy performed on live,
797 immobilized embryos.

798 (**B**) Representative schematic of an embryonic brain. Grey and Red show cerebral
799 arteries and pial collaterals respectively.

800 (**C**) Experimental design to genetically label and trace the dynamics of pre-existing
801 artery endothelial cells in a developing pial layer.

802 (**D**-**G**) Images obtained through macro-zoom fluorescent microscopy of e16.5
803 embryos. In black are cells derived from pre-existing artery endothelial cells. Images
804 were taken by focusing in and out to capture the entire curvature of the embryonic
805 brain. **D** shows an entire left hemisphere. **E** represents watershed region spanned by
806 MCA and ACA artery tips and imaged at time=0 minutes, 20 minutes and 80 minutes
807 respectively. Arrows and arrowheads show growing ends of pre-existing artery tips
808 from MCA and ACA. Brackets mark regions where collaterals appear. **F** shows inset
809 in **D**. **E** and **G** show insets in **F**. **G** represents the MCA growth front imaged at time=0
810 minutes, 20 minutes and 80 minutes respectively. * shows a superficial yolk sac
811 vessel which photobleaches with time. Arrowheads mark extension and
812 anastomoses of MCA artery tips.

813 (**H**-**J**) Images obtained through confocal microscopy from e16 embryos. **H** shows pial
814 watershed and the cerebral arteries spanning the watershed. **I**, **J** show MCA and
815 ACA growth fronts respectively imaged at time=0 minutes and 60 minutes. In black

816 are cells derived from pre-existing artery endothelial cells. Images shown in **I** are
817 maximum intensity projections from 50 optical slices and capture the entire width of
818 the artery. Images shown in **J** are maximum intensity projections from 40 optical
819 slices and capture the entire width of the artery * represents an internal landmark
820 from where the length measurements were done.

821 (**K**) Confocal images of e17 pial layer showing presence of TdTomato$^+$ pre-existing
822 artery endothelial cells (arrowheads) on eGFP$^+$ microvascular tracks. Arrowheads
823 point to TdTomato$^+$ artery cells (red) on microvascular tracks (green).

824 (**L**) A model proposing extension of artery tips along microvascular tracks which
825 leads to pial collateral formation during embryogenesis. Red arrows point to the
826 direction of artery tip elongation. MCA, Middle cerebral artery; ACA, Anterior cerebral
827 artery; e, embryonic day; Tam, Tamoxifen; EC, endothelial cell; YSV, yolk sac
828 vessel; brch., branch; coll, collateral; MV, microvascular. Scale bars: **D**, **F** 1mm; **E**, **G**
829 200 μm; **H**, 500 μm; **I**, **J**, **K** 100 μm.

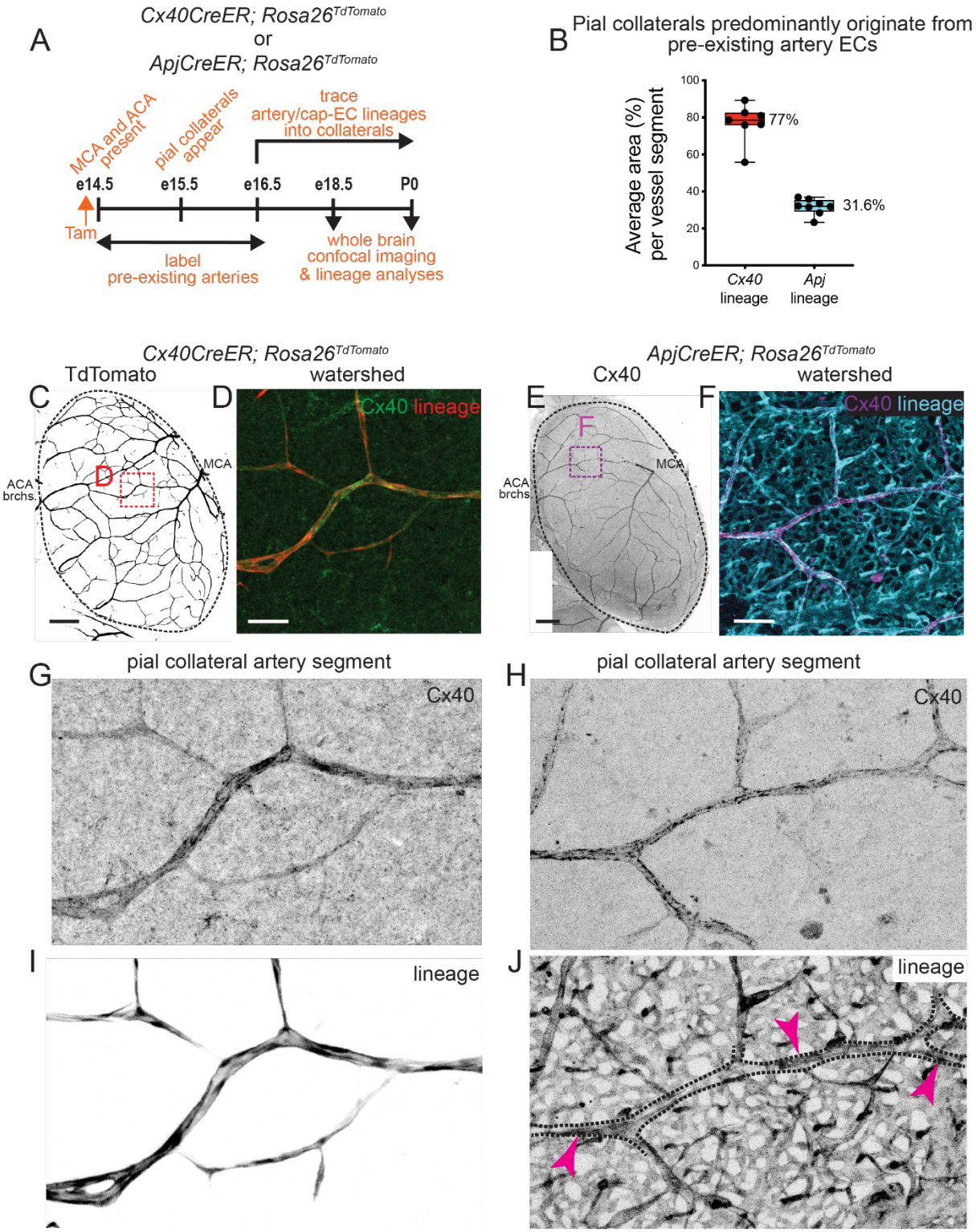


830

831

832

833

834 **Figure 2: Cellular origin of pial collaterals**

835 (**A**) Experimental design to assess lineage contribution from artery ECs and capillary
836 ECs towards pial collaterals at e18.5/ P0.
837 (**B**) Graph shows the average percent area of collateral segments covered with
838 TdTomato$^{+}$ cells.
839 (**C**) Representative image of whole right hemisphere from *Cx40CreER*;
840 *Rosa26$^{TdTomato}$* e18.5 embryos. Black shows TdTomato$^{+}$ arteries.
841 (**D**) Boxed region of interest with a collateral segment from the watershed area
842 shown in **C**. The pial collateral is lineage traced for artery ECs (red) and
843 immunostained with Cx40 (green).
844 **(E**) Representative image of whole right hemisphere from *ApjCreER*; *Rosa26$^{TdTomato}$*
845 e18.5 embryos. Black shows Cx40 immunostaining.
846 (**F**) Boxed region of interest with a collateral segment from the watershed area
847 shown in **E**. The pial collateral is lineage traced for capillary ECs (magenta) and
848 immunostained with Cx40 (cyan).
849 (**G**, **I**) Collateral segment from **D** is (**G**) immunostained for Cx40 and (**I**) lineage
850 traced with TdTomato.
851 (**H**, **J**) Collateral segment from **F** is (**H**) immunostained for Cx40 and (**J**) lineage
852 traced with TdTomato. Arrowheads point to TdTomato$^{+}$ cells from Apj$^{+}$ lineage on the
853 collateral segment. e, embryonic day, P, postnatal day; MCA, Middle cerebral artery;
854 ACA, Anterior cerebral artery; brch., branch; EC, endothelial cell. Scale bars: **C** and
855 **E**, 500μm; **D** and **F**, 100μm
856

857

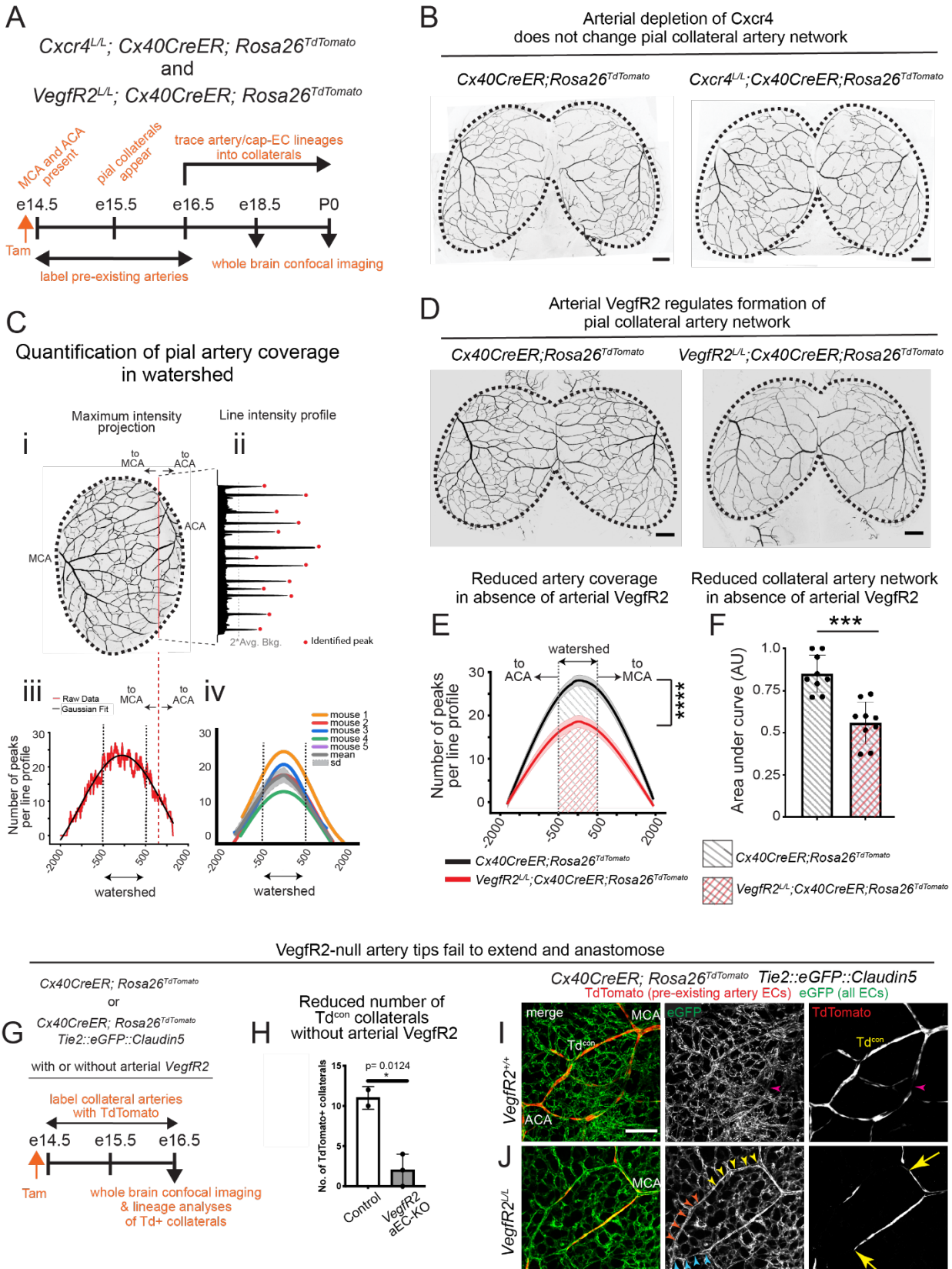
A
Cxcr4L/L; Cx40CreER; Rosa26TdTomato
and
VegfR2L/L; Cx40CreER; Rosa26TdTomato
MCA and ACA present
pial collaterals appear
trace artery/cap-EC lineages into collaterals
e14.5
e15.5
e16.5
e18.5
P0
Tam
label pre-existing arteries
whole brain confocal imaging
B
Arterial depletion of Cxcr4 does not change pial collateral artery network
Cx40CreER;Rosa26TdTomato
Cxcr4L/L;Cx40CreER;Rosa26TdTomato
C
Quantification of pial artery coverage in watershed
Maximum intensity projection
Line intensity profile
i
ii
to MCA
to ACA
MCA
ACA
2*Avg. Bkg.
Identified peak
iii
iv
Raw Data
Gaussian Fit
Number of peaks per line profile
watershed
mouse 1
mouse 2
mouse 3
mouse 4
mouse 5
mean
sd
D
Arterial VegfR2 regulates formation of pial collateral artery network
Cx40CreER;Rosa26TdTomato
VegfR2L/L;Cx40CreER;Rosa26TdTomato
Reduced artery coverage in absence of arterial VegfR2
Reduced collateral artery network in absence of arterial VegfR2
E
F
****
***
Area under curve (AU)
Cx40CreER;Rosa26TdTomato
VegfR2L/L;Cx40CreER;Rosa26TdTomato
VegfR2-null artery tips fail to extend and anastomose
Cx40CreER; Rosa26TdTomato
or
Cx40CreER; Rosa26TdTomato
Tie2::eGFP::Claudin5
with or without arterial VegfR2
G
label collateral arteries with TdTomato
e14.5
e15.5
e16.5
Tam
whole brain confocal imaging & lineage analyses of Td+ collaterals
H
Reduced number of Tdcon collaterals without arterial VegfR2
p= 0.0124
No. of TdTomato+ collaterals
Control
VegfR2 aEC-KO
Cx40CreER; Rosa26TdTomato Tie2::eGFP::Claudin5
TdTomato (pre-existing artery ECs) eGFP (all ECs)
I
J
merge
MCA
ACA
eGFP
TdTomato
Tdcon
VegfR2+/+
VegfR2L/L

858

859

860 **Figure 3: VegfR2-dependent formation of pial collateral arteries**

861 (**A**) Experimental design to lineage label and trace pre-existing artery endothelial
862 cells in pial layer, with or without arterial *VegfR2* and *Cxcr4* at e18.5/ P0.

863 (**B**) Representative confocal images of whole brains with and without arterial *Cxcr4*.
864 Black shows pre-existing artery endothelial cells. Control= 8, artery specific knockout
865 for *Cxcr4*= 13.

866 (**C**) Summary of method to quantify pial artery coverage across the entire brain
867 including watershed.

868 (**D**) Confocal images of whole brains with and without arterial *VegfR2*. Black shows
869 pre-existing artery endothelial cells.

870 (**E**) Quantification of overall pial artery coverage with and without arterial *VegfR2*
871 quantified using method shown in **C**. KS test performed on the distributions
872 generated D value= 0.569, p value= $2.2066 \times 10^{-141}$.

873 (**F**) Quantification of pial collateral artery network with and without arterial *VegfR2*
874 quantified using method shown in **C**. Unpaired t-test, p=0.0001.

875 (**G**) Experimental design to assess the effect of *VegfR2* deletion from arteries at
876 e16.5. (**H**) Quantification of pial collateral arteries contiguously populated with
877 TdTomato$^{+}$ artery cells, with and without arterial *VegfR2*. (**I**, **J**) Confocal images of
878 pial watershed region showing TdTomato-contiguous pial collateral arteries (Td$^{con}$) in
879 red and microvasculature in green. Arrowheads show part of microvascular track not
880 occupied by TdTomato$^{+}$ artery cell, arrows point to artery tips on microvascular
881 tracks. MCA, Middle cerebral artery; ACA, Anterior cerebral artery; e, embryonic day;
882 P, postnatal day; Tam, Tamoxifen; EC, endothelial cell; Td$^{con}$, TdTomato-contiguous;

883 AU, Arbitrary Unit; aEC, artery endothelial cell; KO, knockout. Scale bars: **B**, **D**,

884 500μm; **I**, **J**, 100μm.

885

886

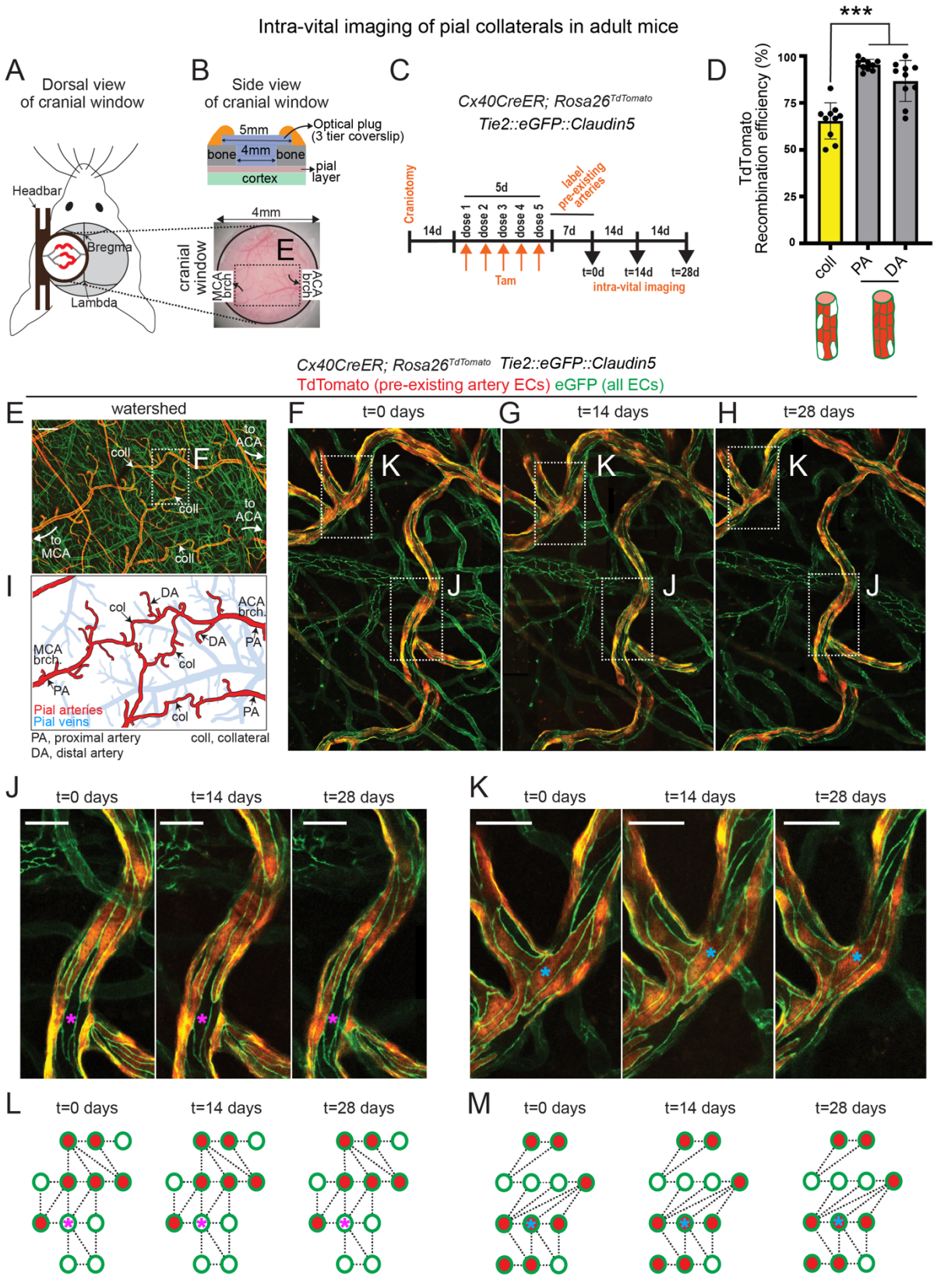
Intra-vital imaging of pial collaterals in adult mice
A
Dorsal view of cranial window
Headbar
Bregma
Lambda
B
Side view of cranial window
5mm
4mm
bone
bone
cortex
Optical plug (3 tier coverslip)
pial layer
4mm
cranial window
MCA brch
ACA brch
E
C
Cx40CreER; Rosa26TdTomato
Tie2::eGFP::Claudin5
Craniotomy
14d
5d
dose 1
dose 2
dose 3
dose 4
dose 5
Tam
label pre-existing arteries
7d
14d
14d
t=0d
t=14d
t=28d
intra-vital imaging
D
***
TdTomato Recombination efficiency (%)
100
75
50
25
0
coll
PA
DA
Cx40CreER; Rosa26TdTomato Tie2::eGFP::Claudin5
TdTomato (pre-existing artery ECs) eGFP (all ECs)
E
watershed
coll
F
to ACA
coll
to ACA
to MCA
coll
I
DA
col
ACA brch.
DA
PA
MCA brch.
col
PA
Pial arteries
Pial veins
col
PA
PA, proximal artery
DA, distal artery
coll, collateral
F
t=0 days
G
t=14 days
H
t=28 days
K
J
J
t=0 days
t=14 days
t=28 days
K
t=0 days
t=14 days
t=28 days
L
t=0 days
t=14 days
t=28 days
M
t=0 days
t=14 days
t=28 days

887

888

889

890 **Figure 4: Longitudinal live-imaging of adult pial collaterals**

891 (**A**, **left**) Dorsal view of the cranial window created with the attached headbar on
892 adult mouse head. (**A**, **right**) Brightfield image of the 4mm cranial window obtained
893 with a stereoscope shows the pial vasculature. Dotted rectangle encompasses MCA,
894 ACA and the watershed between them and is imaged at high resolution as shown in
895 **E**.

896 (**B**) Schematic of the side view of the cranial window showing the 3-tier optical plug
897 inserted into the skull giving access to pial layer.

898 (**C**) Experimental design for longitudinal imaging of pial vasculature in adult mice.

899 (**D**) Quantification of TdTomato reporter recombination in pial collateral arteries and
900 different segments of cerebral arteries. One-way ANOVA was done to test
901 significance statistically (mean comparison Tukey test, PA vs. collateral, $p<0.0001$;
902 DA vs. collateral, $p<0.0001$; PA vs. DA, $p=0.08$).

903 (**E**-**K**) Images of pial watershed with pre-existing artery endothelial cells labelled in
904 TdTomato (red) and all endothelial cells labelled in eGFP (green). (**E**) Confocal
905 image from optical window created for longitudinal imaging of *Cx40CreER;*
906 *Rosa26$^{TdTomato}$; Tie2::eGFP::Claudin5* mouse as shown in Figure **4A**. The image
907 shows both pial and dural vessels. (**F**-**K**) Confocal images of pial collateral arteries
908 from cranial window shown in **E**, across 3 timepoints, each 2 weeks apart. (**I**) Pial
909 layer segmented out from **E**. red and blue show pial arteries and veins respectively.
910 **J**, **K** are the insets shown in **F**-**H**.

911 (**L**, **M**) Cellular distribution of TdTomato+ artery cells and eGFP+ endothelial cells in
912 collateral artery segments shown in **J** and **K** respectively. * represents a reference

913 cell. MCA, middle cerebral artery; ACA, anterior cerebral artery; d, days; Tam,

914 Tamoxifen; PA, proximal artery; DA, distal artery; coll, collateral; brch., branch; EC,

915 endothelial cell. Scale bars: **E**, 200μm; **J**, **K** 25μm

916

Intra-vital imaging of VegfR2 deficient pial collaterals in adult mice

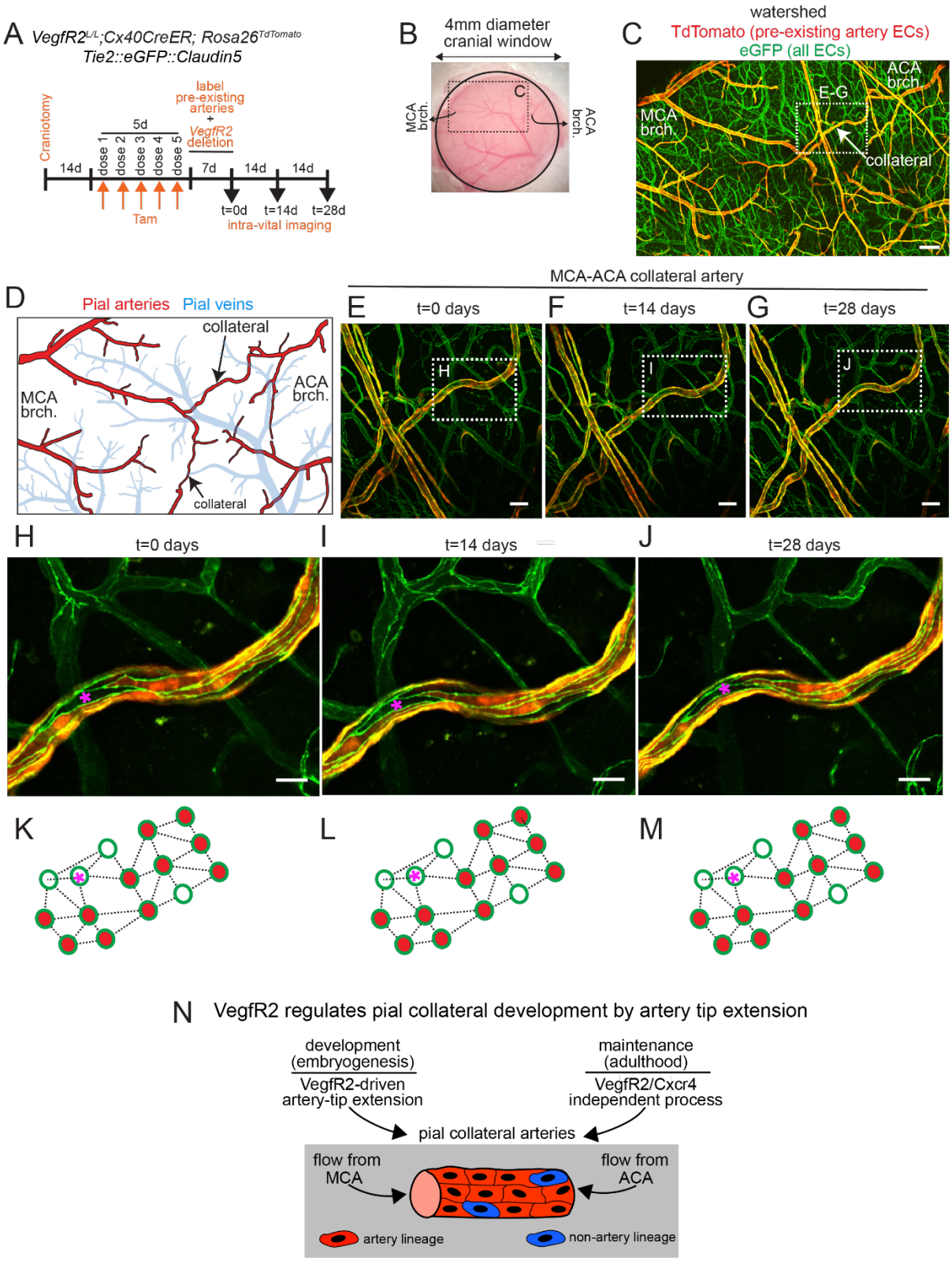


917

918

919

920 **Figure 5: Analyses of role of arterial VegfR2 in pial collateral maintenance**

921 **(A)** Experimental design to visualize artery cell dynamics in pial layer of adult mice
922 without arterial *VegfR2*.

923 (**B**) Brightfield image of cranial window showing pial vasculature. The dotted
924 rectangle encompasses branches of MCA, ACA and the watershed between them.

925 (**C**) Confocal image of cranial window created in mice without arterial *VegfR2* as
926 shown in **B**. Red shows all artery cells, green shows all endothelial cells.

927 (**D**) Pial layer segmented out from **C** shows pial arteries and veins in red and blue
928 respectively.

929 (**E**-**G**) Confocal images of collateral artery from three timepoints, each 2 weeks apart
930 as shown in the boxed region in **C**.

931 (**H**-**J**) Confocal images of collateral artery segments shown in **E**-**G**.

932 (**K**-**M**) Cellular distribution of TdTomato$^{+}$ artery cells and eGFP$^{+}$ endothelial cells in
933 collateral artery segments shown in **H**-**J**. * represents a reference cell.

934 (**N**) Schematic summarizing the role of arterial VegfR2 in development and
935 maintenance of pial collateral arteries. While arterial VegfR2 facilitates tip extension
936 of pre-existing arteries during development, it is dispensable for pial collateral
937 maintenance in adulthood. Pial collaterals, both in developing and mature brains, are
938 majorly populated by endothelial cells of artery-lineage. MCA, middle cerebral artery;
939 ACA, anterior cerebral artery; d, days; Tam, Tamoxifen; EC, endothelial cell; brch.,
940 branch. Scale bars: **C**, 150 μm; **E**-**G**, 50μm; **H**-**J**, 20μm.

941

942 **Supplementary figures and figure legends**

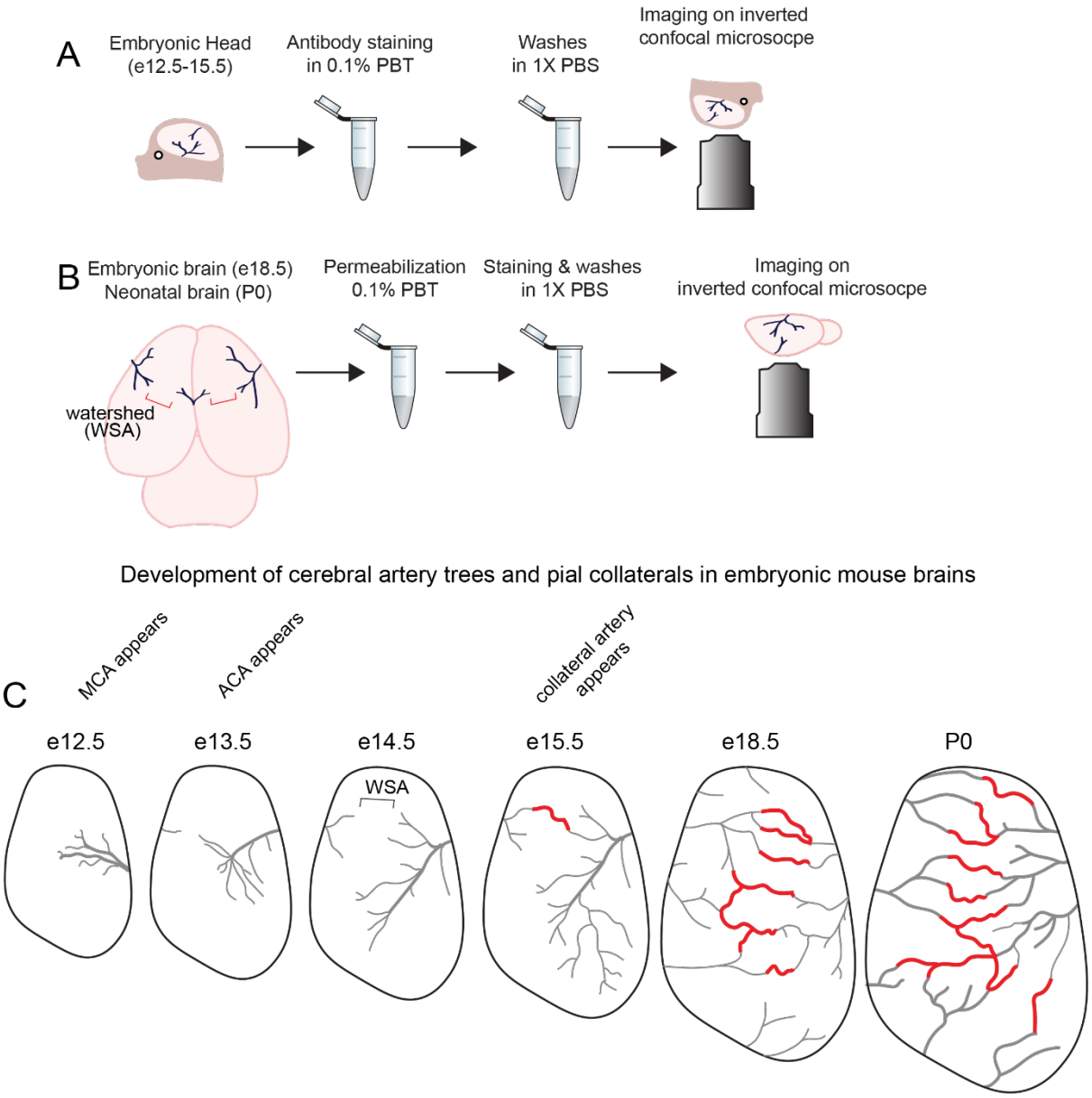


943

944

945

946

947

948

949 **Supplemental Figure 1: Visualization of pial arteries and collateral arteries**

950 Schematic summarizes key steps of immunostaining methods used to image pial
951 artery network in (**A**) mouse embryonic heads and (**B**) mouse embryonic/neonatal
952 brains with confocal microscope. (**C**) Schematic shows findings from **A** and **B** in one
953 hemisphere. Grey represents cerebral arteries, Red represents collateral artery
954 connections between cerebral arteries. Brackets show watershed area (WSA), MCA
955 appears at e12.5, ACA appears at e13.5, and the foremost pial collateral arteries
956 appear at e15.5. These pial collaterals then increase in number till e18.5/P0. e,
957 embryonic; P, postnatal day; MCA, middle cerebral artery; ACA, anterior cerebral
958 artery.

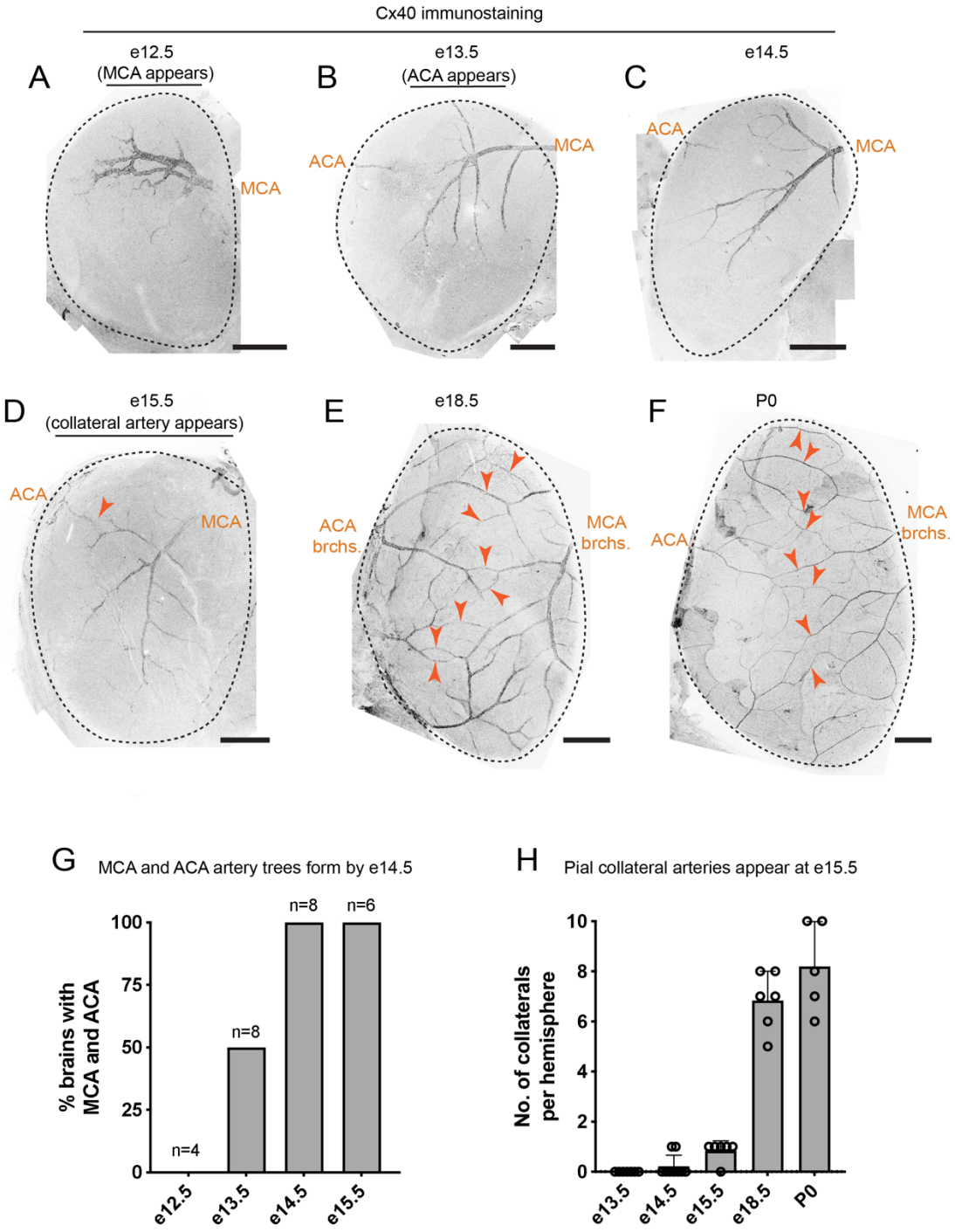
Cx40 immunostaining
A
e12.5
(MCA appears)
MCA
B
e13.5
(ACA appears)
ACA
MCA
C
e14.5
ACA
MCA
D
e15.5
(collateral artery appears)
ACA
MCA
E
e18.5
ACA
brchs.
MCA
brchs.
F
P0
ACA
MCA
brchs.
G
MCA and ACA artery trees form by e14.5
% brains with
MCA and ACA
100
75
50
25
0
n=4
n=8
n=8
n=6
e12.5
e13.5
e14.5
e15.5
H
Pial collateral arteries appear at e15.5
No. of collaterals
per hemisphere
10
8
6
4
2
0
e13.5
e14.5
e15.5
e18.5
P0

963 **Supplemental Figure 2: Detection of pial collaterals with whole brain**
964 **immunostaining**

965 (**A**-**F**) Representative images of right hemispheres from developing mouse embryos
966 immunostained for Connexin-40 (Cx40). Cx40 marks all artery endothelial cells.
967 MCA appears at e12.5, ACA appears at e13.5 and collaterals between MCA and
968 ACA appear at e15.5. Arrowheads point to collateral arteries between MCA and
969 ACA. (**G**) Quantification of Cx40 immunostained brains from different developmental
970 stages reveals that both MCA and ACA have formed by e14.5. (**H**) Quantification of
971 $Cx40^{+}$ collateral arteries per hemisphere shows that the first pial collaterals appear at
972 e15.5. e, embryonic; P, postnatal day; MCA, middle cerebral artery; ACA, anterior
973 cerebral artery; brch., branch. Scale bars: 500µm

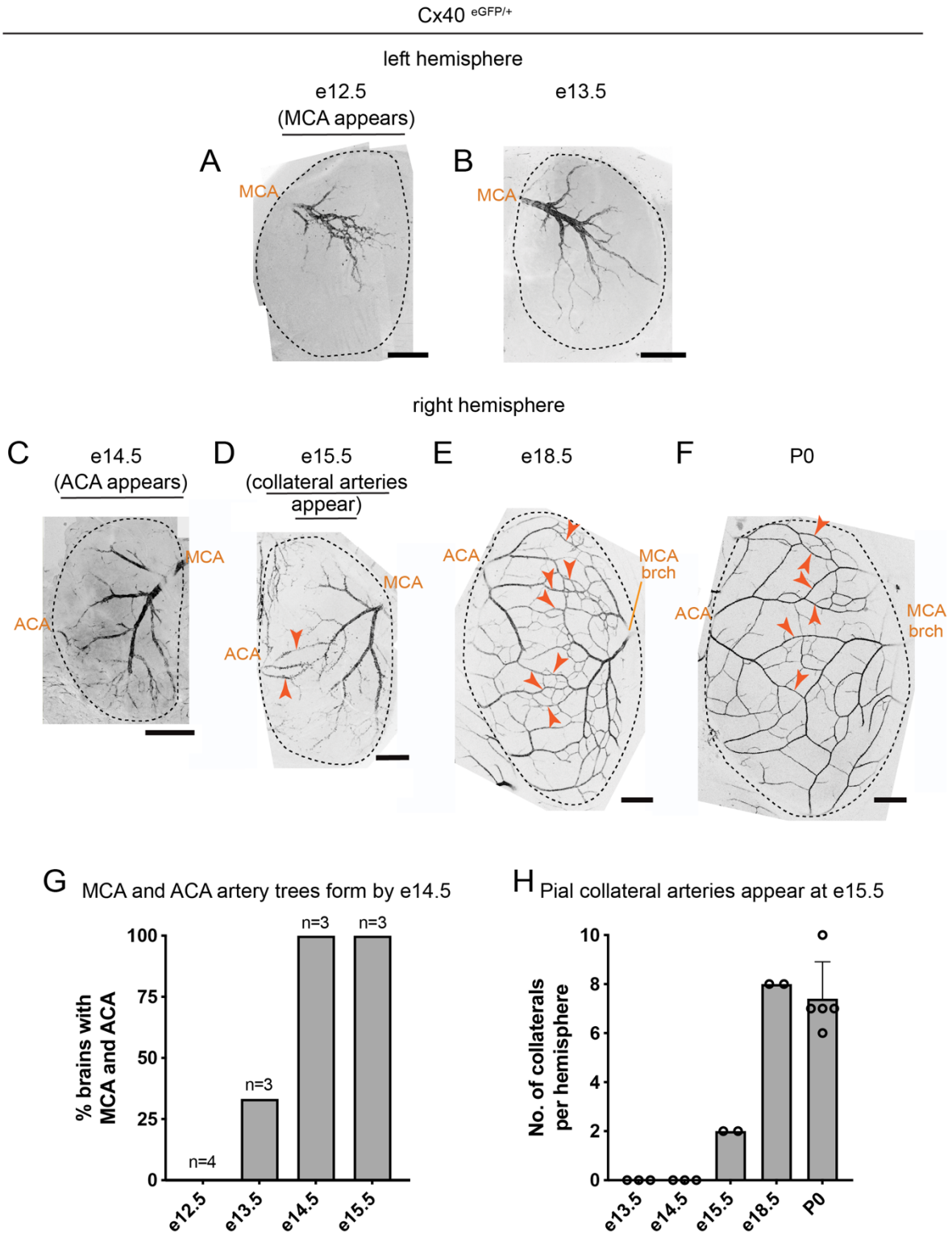
Cx40 eGFP/+
left hemisphere
e12.5
(MCA appears)
e13.5
A
B
MCA
MCA
right hemisphere
C
e14.5
(ACA appears)
D
e15.5
(collateral arteries
appear)
E
e18.5
F
P0
MCA
ACA
MCA
ACA
ACA
MCA
brch
ACA
MCA
brch
G
MCA and ACA artery trees form by e14.5
% brains with
MCA and ACA
100
75
50
25
0
n=4
n=3
n=3
n=3
e12.5
e13.5
e14.5
e15.5
H
Pial collateral arteries appear at e15.5
No. of collaterals
per hemisphere
10
8
6
4
2
0
e13.5
e14.5
e15.5
e18.5
P0

978 **Supplemental Figure 3: Detection of pial collaterals with *Cx40* reporter activity**

979 (**A**-**F**) Representative images of brains from developing *Cx40*$^{eGFP/+}$ mouse embryos.
980 Connexin-40 (Cx40) marks all artery endothelial cells. MCA appears at e12.5, ACA
981 appears at e14.5 and collaterals between MCA and ACA appear at e15.5.
982 Arrowheads point to collateral arteries between MCA and ACA. (**G**) Quantification of
983 *Cx40*$^{eGFP/+}$ brains from different developmental stages reveals that both MCA and
984 ACA have formed by e14.5. (**H**) Quantification of eGFP$^{+}$ collateral arteries per
985 hemisphere shows that the first pial collaterals appear at e15.5. e, embryonic; P,
986 postnatal day; MCA, middle cerebral artery; ACA, anterior cerebral artery; brch.,
987 branch. Scale bars: 500μm

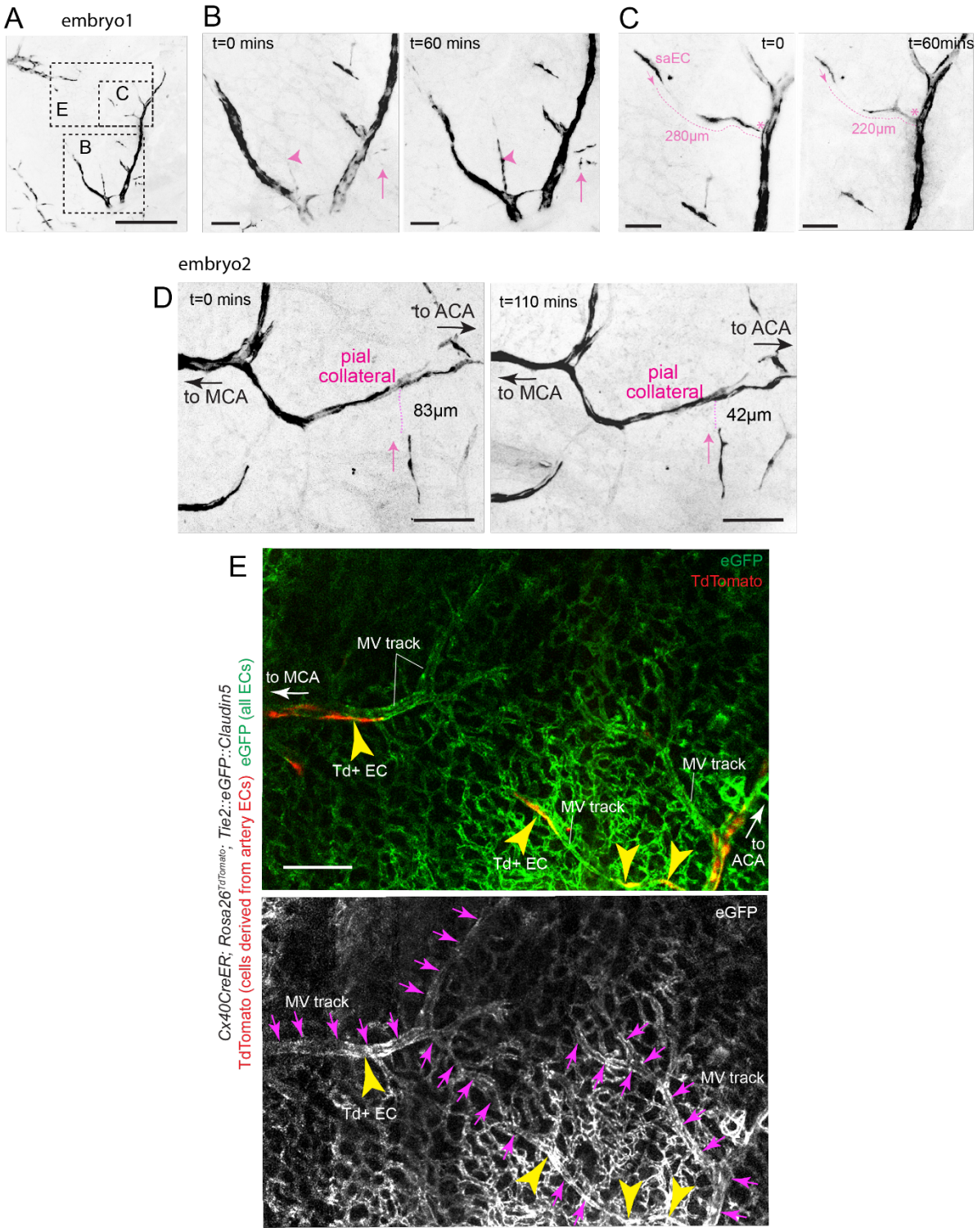


**Supplemental Figure 4: Visualization of pial artery cell dynamics on microvascular tracks** (**A**) Confocal image showing watershed region between MCA and ACA of a live e16 embryo. (**B**, **C**) Insets from **A** showing growth of ACA in 60 mins. In **B**, arrowhead point to an artery tip emerging within 60mins. Arrow points to

993 single artery cells. In **C**, arrow shows direction of migration of single artery cell.
994 Dotted line is the length of micro-vessel between the single cell and the pial artery. *
995 shows a reference point from which measurements were done. (**D**) Confocal image
996 of another e16 embryonic collateral zone showing single artery endothelial cell
997 migration towards the pial collateral within 110mins. Dotted line is the length of
998 micro-vessel between the single cell and the pial collateral. Arrow shows direction of
999 single artery cell migration. (**E**) Inset from **A** showing presence of TdTomato$^{+}$ artery
1000 endothelial cells (yellow arrowheads) on eGFP$^{+}$ microvascular tracks (magenta
1001 arrows). MCA, Middle Cerebral Artery; ACA, Anterior Cerebral Artery; MV,
1002 Microvascular; Td, TdTomato; EC, Endothelial cell. Scale bars: **A**, 500μm; **B**-**E**,
1003 100μm.

1004

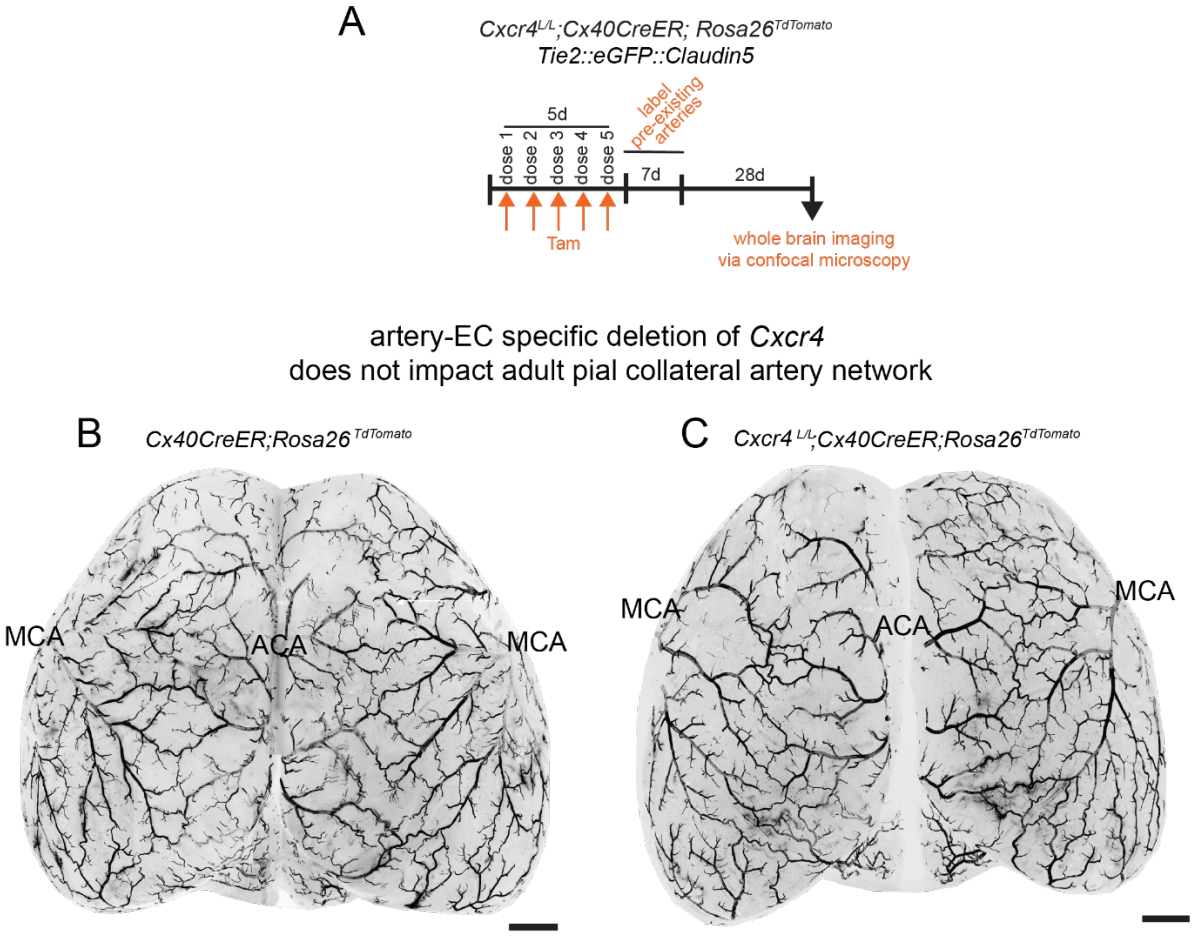


1005

1006

1007

1008

1009

1010

1011

1012

1013

1014 **Supplemental Figure 5: Pial artery coverage does not change without arterial**
1015 ***Cxcr4*** (**A**) Experimental set up to assess the effect of arterial *Cxcr4* deletion on pial
1016 artery coverage in adults. (**B**, **C**) Representative confocal images of whole adult
1017 brains (from N=5 for each genotype), genetically lineage traced for pre-existing
1018 artery endothelial cells, (**B**) with or (**C**) without arterial *Cxcr4*. ACA, anterior cerebral
1019 artery; MCA, middle cerebral artery. Scale bars: 1mm

1020

1021

1022

1023

1024

1025

1026

1027

1028

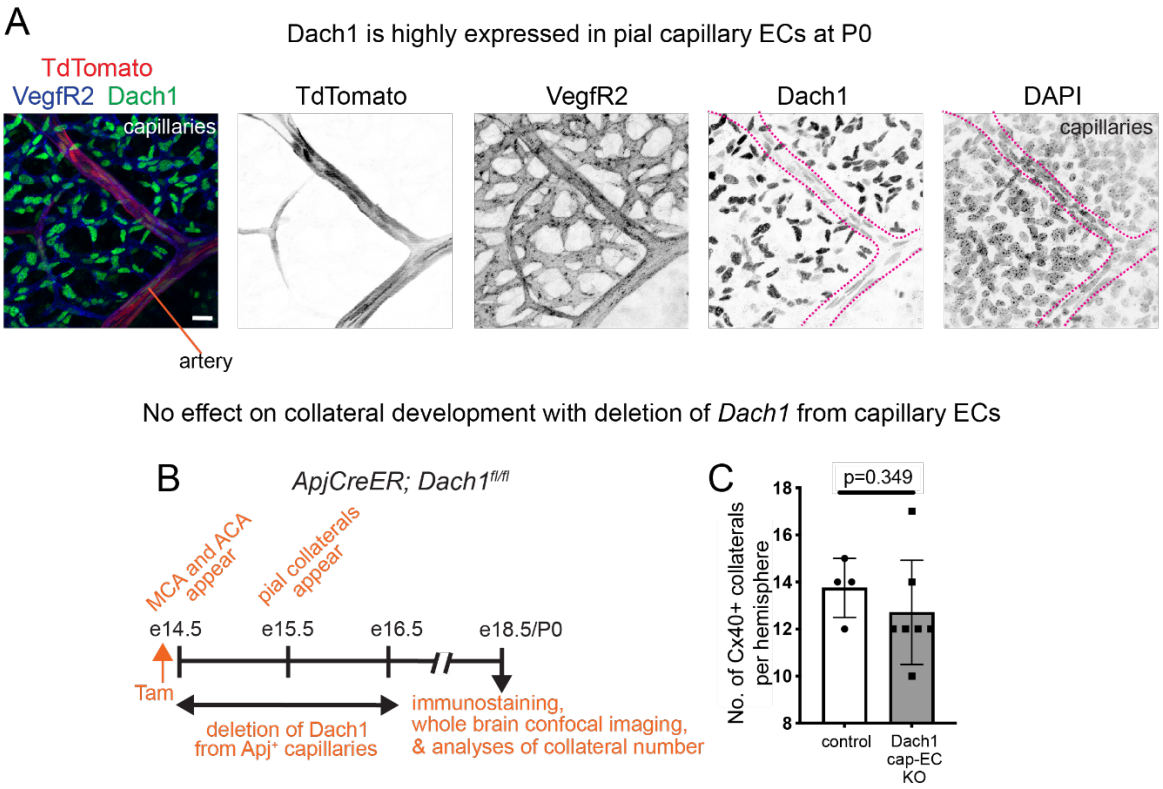


1029

1030

1031

1032

1033

1034

1035

1036

1037

1038

1039

1040 **Supplemental Figure 6: Dach1-independent pial collateral development** (**A**)
1041 Dach1 expression (green) in capillaries and arteries in P0 brains. Dotted line marks
1042 the TdTomato$^{+}$ (red) arterial boundary. VegfR2 marks all vasculature. DAPI marks
1043 nuclei. (**B**) Experimental design showing Tamoxifen injection at e14.5, and analyses
1044 of collateral numbers in e18.5/P0 brains. (**C**) Quantification of Cx40$^{+}$ pial collaterals
1045 between MCA and ACA in control (*Dach1*$^{fl/fl}$) and *ApjCreER*; *Dach1*$^{fl/fl}$ (Dach1 cap-
1046 EC KO) brains. e, embryonic; cap-EC, capillary endothelial cell; KO, knockout. Scale
1047 bar: 20μm.

1048

Intra-vital imaging of VegfR2 deficient pial collaterals in adult mice

*VegfR2*$^{L/L}$ *Cx40CreER; Rosa26*$^{TdTomato}$
*Tie2::eGFP::Claudin5*
TdTomato (pre-existing artery ECs) eGFP (all ECs)

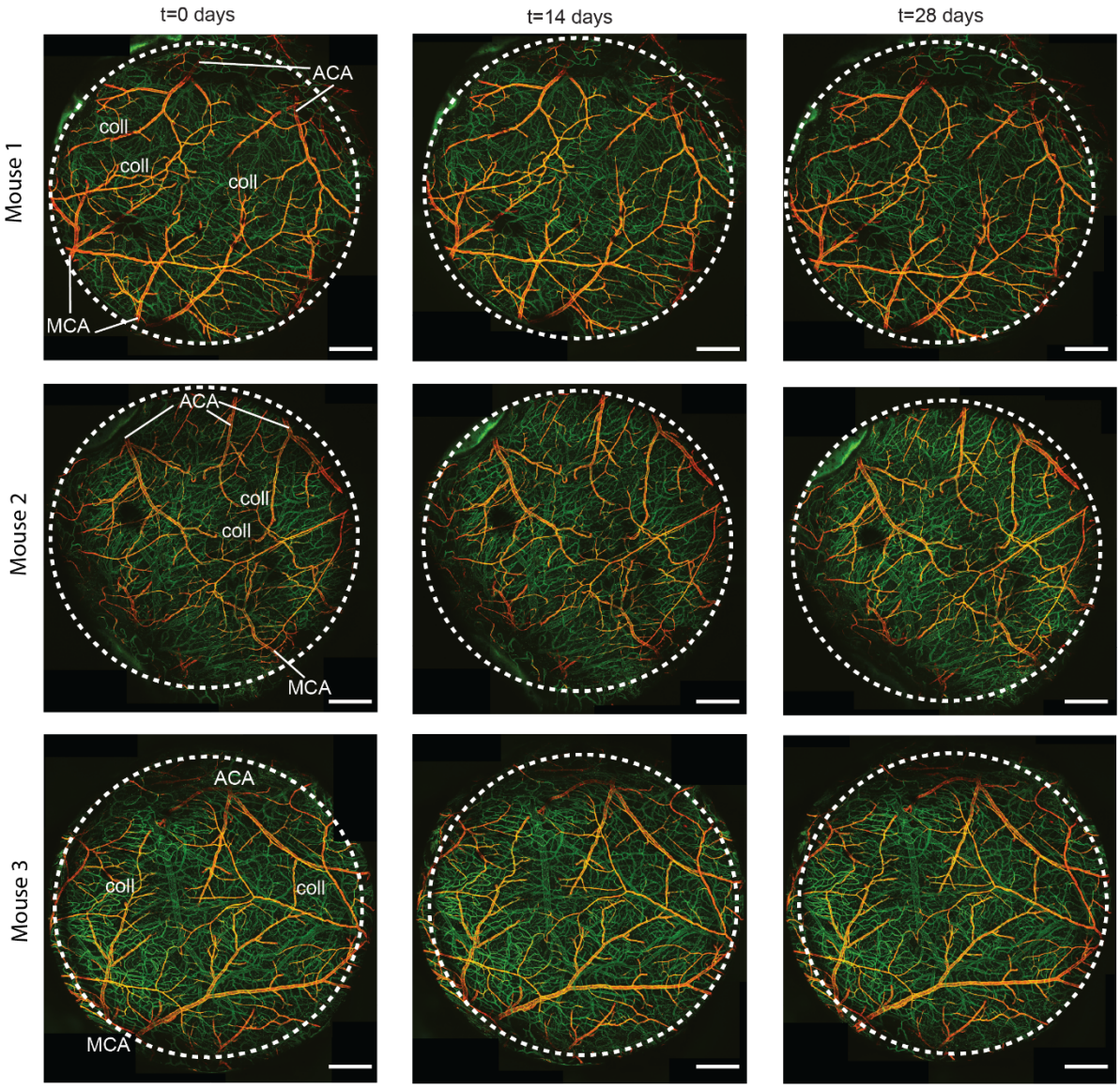


1049

1050

1051

1052

1053

1054

1055 **Supplemental Figure 7: VegfR2-independent maintenance of pial collaterals**

1056 Confocal images of the entire cranial window from 3 different mice shows that the
1057 overall pial artery network remains unchanged without arterial *VegfR2*. MCA, Middle
1058 Cerebral Arteries, ACA, Anterior Cerebral Arteries, Coll, Pial collateral arteries
1059 between MCA and ACA. Scale bars: 500μm.